Journal of the Mechanics and Physics of Solids 115 (2018) 30–53

Contents lists available at ScienceDirect

Journal of the Mechanics and Physics of Solids

journal homepage: www.elsevier.com/locate/jmps

A theory for fracture of polymeric gels

Yunwei Mao, Lallit Anand*

Department of Mechanical Engineering, Massachusetts Institute of Technology, 77 Massachusetts Avenue, Cambridge, MA 02139, United States

ARTICLE INFO

Article history:
Received 27 October 2017
Revised 12 February 2018
Accepted 19 February 2018
Available online 27 February 2018

Keywords:
Polymer gels
Diffusion
Deformation
Chain-scission
Fracture

ABSTRACT

A polymeric gel is a cross-linked polymer network swollen with a solvent. If the concentration of the solvent or the deformation is increased to substantial levels, especially in the presence of flaws, then the gel may rupture. Although various theoretical aspects of coupling of fluid permeation with large deformation of polymeric gels are reasonably well-understood and modeled in the literature, the understanding and modeling of the effects of fluid diffusion on the damage and fracture of polymeric gels is still in its infancy. In this paper we formulate a thermodynamically-consistent theory for fracture of polymeric gels — a theory which accounts for the coupled effects of fluid diffusion, large deformations, damage, and also the gradient effects of damage. The particular constitutive equations for fracture of a gel proposed in our paper, contain two essential new ingredients: (i) Our constitutive equation for the change in free energy of a polymer network accounts for not only changes in the entropy, but also changes in the internal energy due the stretching of the Kuhn segments of the polymer chains in the network. (ii) The damage and failure of the polymer network is taken to occur by chain-scission, a process which is driven by the changes in the internal energy of the stretched polymer chains in the network, and not directly by changes in the configurational entropy of the polymer chains. The theory developed in this paper is numerically implemented in an open-source finite element code MOOSE, by writing our own application. Using this simulation capability we report on our study of the fracture of a polymeric gel, and some interesting phenomena which show the importance of the diffusion of the fluid on fracture response of the gel are highlighted.

1. Introduction

There are numerous polymeric materials which have a crosslinked network and which can absorb large quantities of suitable fluids without the essential skeletal network structure of the polymer being disrupted by the absorbed fluid. Such a polymeric network, together with the fluid molecules, forms a swollen aggregate called a polymeric gel. When the fluid is water, the gel is known as a hydrogel. Gels may be designed to swell by several hundred percent, and — depending on the precise constitution of a gel — the amount of swelling may be controlled by varying external stimuli. Stimuli-responsive polymeric gels have the ability to swell and deswell in response to changes in the environmental conditions such as mechanical forces, temperature, solvent-type, pH, electric field, and also light. Because of their unique characteristics, polymer gels are found in several diverse applications, such as carriers for drug delivery, scaffolds for tissue engineering, soft actuators, smart optical systems, as well as packers for sealing in oil-wells. Living organisms are largely made of polymer gels;

* Corresponding author.
E-mail address: anand@mit.edu (L. Anand).

https://doi.org/10.1016/j.jmps.2018.02.008
0022-5096/

this facilitates the transport of ions and molecules within the organism while keeping its solidity (shape). Hydrogels are commonly considered as proxies for soft biological tissues and are thus the subject of intense theoretical and experimental investigations.

There have been several (essentially-similar) recent publications regarding modeling of the coupled diffusion-deformation response of polymeric gels (Chester and Anand, 2010; Doi, 2009; Duda et al., 2010; Hong et al., 2008). Several papers related to the numerical implementation of these theories for solving coupled diffusion-deformation boundary value problems for gels have also been recently published (Broger et al., 2017a; Chester and Anand, 2011; Chester et al., 2015; Lucantonio et al., 2013).

In order to develop a robust simulation capability for the use of polymer gels in applications, one also needs to be able to model the damage and fracture of these materials. A difficulty in modeling the fracture of gels comes from the influence of the amount of fluid on the propensity to fracture of a gel. Generally, an inhomogeneous deformation field induces an inhomogeneous chemical potential field, which leads to an inhomogeneous concentration of the fluid because of diffusion within the body; such an inhomogeneous fluid concentration leads to an inhomogeneous propensity to fracture within the body. According to the classical arguments of Lake and Thomas (1967), regions of higher fluid concentration (and therefore lower polymer volume fraction) have an increased propensity to damage and failure because of the lower number of highly stretched polymer chains. Further, because of the diffusion, the damage process zone in the vicinity of a crack — when compared to the overall geometry of a body — is not always small, and classical notions of "small-scale process zone" often do not hold. The heterogenous propensity to fracture and large damage process zones makes classical fracture mechanics criteria — like the energy release rate reaching a critical value — inapplicable. Also, since diffusion of the fluid relative to the polymer network is a dissipative process, classical fracture mechanics models which are based entirely on Lake–Thomas-type energetic arguments, and which do not account for the dissipation due to diffusion, will underestimate the fracture resistance of polymeric gels.

Thus a theory and a numerical simulation capability which couples diffusion of the fluid with the large deformation, damage and fracture of polymeric gels is needed. Most of the existing studies on the fracture of gels have limited their attention to conditions under which the characteristic time-scale for deformation is much smaller than the time-scale for diffusion, so that the diffusion of the fluid may be neglected (Brown, 2007; Tanaka, 2007; Zhang et al., 2015). However, there are many important operating conditions under which the fluid diffusion cannot be ignored. One such set of conditions occurs when a notched-specimen is stretched to a sub-critical level and thereafter the stretch is held constant; after a sufficient incubation time damage initiates, accumulates, and eventually fracture occurs — a phenomenon known as "delayed-fracture"; this phenomenon cannot be explained by ignoring the diffusion of the fluid (Bonn et al., 1998; Tang et al., 2017; Wang and Hong, 2012).

There are very few papers in the literature which address the complete coupled diffusion-deformation-fracture problems in gels; the only paper that we are aware of is the very recent paper of Broger et al. (2017b). In their paper these authors propose a diffusion-deformation-fracture theory with a diffuse-crack approximation based on a phase-field/damage variable d.[1] They present a variational framework for their phase-field fracture theory of gels together with a numerical implementation of their variational theory in a finite element program, and show some interesting simulations of crack initiation and propagation during drying of hydrogels. For other previous papers on fracture of polymer gels — papers which are based on generalizations of classical fracture mechanics theories and not on phase-field or gradient-damage theories — see, e.g., Wang and Hong (2012), Hui et al. (2013), Bouklas et al. (2015), and Noselli et al. (2016).

The purpose of our paper is also to address the coupled diffusion-deformation-fracture problem for an "ideal" single-network polymeric gel. If the cross-linking chemical bonds in such a network are strong then fracture is expected to occur by scission of the chains between the crosslinks, as envisioned in the classical model of Lake and Thomas (1967), while if the chemical crosslinks are weak then fracture is expected to occur because of the scission of the cross-linking bonds themselves. In this paper we focus our attention networks with strong cross-linking bonds which fail by chain-scission.[2] Further, as in the theory of Broger et al. (2017b), to model the fracture of a gel we introduce a damage variable $d(\mathbf{X}, t) \in [0, 1]$. If $d = 0$ at a point then that point is intact, while if $d = 1$ at some point, then that point is fractured. Values of d between zero and one correspond to partially-fractured material. We assume that d grows monotonically so that $\dot{d}(\mathbf{X}, t) \geq 0$, which is a constraint that represents the usual assumption that microstructural changes leading to fracture are irreversible. As in Broger et al. (2017b) our theory also accounts for the gradient of the damage variable, ∇d. However, in contrast to the particular "incremental variational" approach taken by these authors in formulating their theory, we formulate our gradient-damage theory by using Gurtin's pioneering virtual-power approach (Gurtin, 1996; 2002). This approach leads to macroforce and microforce balances for the forces associated with the rate-like kinematical descriptors in the theory. These macro- and microforce balances, together with a free-energy imbalance law under isothermal conditions, when supplemented with a set of thermodynamically-consistent constitutive equations, provide the governing equations for our theory. The particular constitutive equations for fracture of a gel in our paper are based on extensions of a physical model of fracture of dry

[1] The origins of the regularization of a sharp crack discontinuity in their diffuse-crack theory may be traced back to the energy minimization concepts of brittle fracture mechanics proposed in Francfort and Marigo (1998) and Bourdin et al. (2000).

[2] We leave a consideration of interpenetrating-multiple-network gels, as well as materials which exhibit additional non-trivial dissipation mechanisms such as viscoelasticity and Mullins-effect, to future efforts.

elastomers presented in our recent papers (Mao et al., 2017b; Talamini et al., 2018) which contain two essential new physical ingredients:

- Our constitutive equation for the change in free energy of a polymer network accounts for not only changes in the entropy, but also changes in the internal energy due to the stretching of the Kuhn segments of the polymer chains in the network. To do so, we introduce a dimensionless positive-valued internal variable, $\lambda_b \in [1, \infty)$, to represent (at the continuum scale) a measure of the stretch of the Kuhn segments. We call λ_b the effective bond stretch.
- The damage and failure of a polymer network with strong cross-linking chemical bonds is taken to occur by chain-scission, a process which is driven by the changes in the internal energy of the stretched polymer chains in the network, and not (directly) by changes in the configurational entropy of the polymer chains.

The paper by Broger et al. (2017b) does not consider changes in the internal energy of a polymer network by stretching of the Kuhn segments. Their model for fracture of a gel is based entirely on changes of free energy due to configurational entropy changes, which we believe is not what occurs physically in a polymer network with strong chemical crosslinks.

The plan of this paper is follows. We begin in Section 2 with the formulation of our continuum-mechanical theory. In Section 3 we specialize the constitutive equations of our theory. The governing equations of the specialized theory are summarized in Section 4. The theory developed in this paper is numerically implemented in an open-source finite element code MOOSE (Gaston et al., 2009) by writing our own application. Using this simulation capability, in Section 5 we present results form our simulations of Mode-I fracture in single-edge-notch and asymmetric-double-edge-notch geometries under plane-stress conditions. In Sections 5.1 and 5.2 the single-edge notch geometry is used to explore the consequences of the competition between the characteristic time-scale for deformation and the characteristic time-scale for diffusion by fixing the time scale for deformation, and varying the value of the diffusivity of the fluid. While there are many operating conditions under which the characteristic time-scale for deformation is much smaller than the time-scale for diffusion, so that the diffusion of the fluid may be neglected, there are also operating conditions under which the fluid diffusion cannot be ignored — such as conditions leading to "delayed-fracture", discussed earlier. We numerically study the phenomenon of "delayed-fracture" in Section 5.3, and clarify the important role of fluid diffusion in this phenomenon. In Section 5.4 we report on our study of fracture of an asymmetric-double-notched sheet specimen of a gel under Mode-I plane-stress loading. This example shows the capability of our gradient damage theory and its numerical implementation to model merging of two notches. We close in Section 6 with some final remarks.

2. Theory

2.1. Basic kinematics

Consider a fluid-containing (wet) macroscopically-homogeneous body made from an elastomeric gel. In what follows, the spatially-continuous fields that define our continuum theory represent averages meant to apply at length scales which are large compared to the length scales associated with the molecular network and its microscopic-scale free-volume. We identify such a macroscopically-homogeneous body B with the region of space it occupies in a fixed *reference configuration*, and denote by $\mathbf{X}$ an arbitrary material point of B.[3] A motion of B is a smooth one-to-one mapping $\mathbf{x} = \boldsymbol{\chi}(\mathbf{X}, t)$ with deformation gradient, velocity, and velocity gradient given by

$$\mathbf{F} = \nabla \boldsymbol{\chi}, \quad \mathbf{v} = \dot{\boldsymbol{\chi}}, \quad \mathbf{L} = \operatorname{grad} \mathbf{v} = \dot{\mathbf{F}}\mathbf{F}^{-1}. \tag{2.1}$$

We base the theory on a multiplicative decomposition of the deformation gradient

$$\mathbf{F} = \mathbf{F}^e\mathbf{F}^s, \tag{2.2}$$

where,

- $\mathbf{F}^s$ represents the local distortion of the material neighborhood of $\mathbf{X}$ due to the insertion/extraction of the fluid molecules due to the diffusion of the fluid; and
- $\mathbf{F}^e$ represents the subsequent stretching and rotation of this coherent fluid-distorted material neighborhood, and thereby represents a corresponding mechanical distortion.

We refer to $\mathbf{F}^s$ and $\mathbf{F}^e$ as the swelling and mechanical distortions, respectively. We write

$$J = \det \mathbf{F} > 0, \tag{2.3}$$

and hence we have

$$J = J^eJ^s, \quad \text{and we assume that} \quad J^e = \det \mathbf{F}^e > 0, \quad \text{and} \quad J^s = \det \mathbf{F}^s > 0, \tag{2.4}$$

[3] Notation: We use standard notation of modern continuum mechanics (Gurtin et al., 2010). Specifically: ∇ and Div denote the gradient and divergence with respect to the material point $\mathbf{X}$ in the reference configuration, and $\Delta = \text{Div}\nabla$ denotes the referential Laplace operator; grad, div, and div grad denote these operators with respect to the point $\mathbf{x} = \boldsymbol{\chi}(\mathbf{X}, t)$ in the deformed body; a superposed dot denotes the material time-derivative. Throughout, we write $\mathbf{F}^{e-1} = (\mathbf{F}^e)^{-1}$, $\mathbf{F}^{e-\top} = (\mathbf{F}^e)^{-\top}$, etc. We write tr $\mathbf{A}$, sym $\mathbf{A}$, skw $\mathbf{A}$, $\mathbf{A}_0$, and $\text{sym}_0\mathbf{A}$ respectively, for the trace, symmetric, skew, deviatoric, and symmetric-deviatoric parts of a tensor $\mathbf{A}$. Also, the inner product of tensors $\mathbf{A}$ and $\mathbf{B}$ is denoted by $\mathbf{A}$: $\mathbf{B}$, and the magnitude of $\mathbf{A}$ by $|\mathbf{A}| = \sqrt{\mathbf{A} : \mathbf{A}}$.

so that $\mathbf{F}^e$ and $\mathbf{F}^s$ are invertible.

The total and elastic right Cauchy–Green deformation tensors are given by

$$\mathbf{C} = \mathbf{F}^\top \mathbf{F} \qquad \text{and} \qquad \mathbf{C}^e = \mathbf{F}^{e\top} \mathbf{F}^e, \tag{2.5}$$

respectively. Next, by the definition $(2.1)_3$, we have

$$\mathbf{L} = \mathbf{L}^e + \mathbf{F}^e \mathbf{L}^s \mathbf{F}^{e-1}, \quad \text{with} \quad \mathbf{L}^e = \dot{\mathbf{F}}^e \mathbf{F}^{e-1}, \quad \text{and} \quad \mathbf{L}^s = \dot{\mathbf{F}}^s \mathbf{F}^{s-1}, \tag{2.6}$$

where $\mathbf{L}^s$ represents a distortion rate due to insertion/extraction of the fluid molecules. As is standard, we define the elastic and swelling stretching and spin tensors through

$$\mathbf{D}^e = \operatorname{sym} \mathbf{L}^e, \qquad \mathbf{W}^e = \operatorname{skw} \mathbf{L}^e, \qquad \mathbf{D}^s = \operatorname{sym} \mathbf{L}^s, \qquad \mathbf{W}^s = \operatorname{skw} \mathbf{L}^s, \tag{2.7}$$

so that $\mathbf{L}^e = \mathbf{D}^e + \mathbf{W}^e$, and $\mathbf{L}^s = \mathbf{D}^s + \mathbf{W}^s$.

We assume that the swelling distortion $\mathbf{F}^s$ is isotropic and given by,

$$\mathbf{F}^s = \lambda^s \mathbf{1}, \qquad \lambda^s = (J^s)^{1/3} > 0; \tag{2.8}$$

we call λ^s the swell-stretch. Further, from the definitions of $\mathbf{D}^s$ and $\mathbf{W}^s$ in (2.7), the definition of $\mathbf{L}^s$ in (2.6), and the specific expression for $\mathbf{F}^s$ in (2.8), we have,

$$\mathbf{D}^s = (\dot{\lambda}^s \lambda^{s-1}) \mathbf{1}, \quad \text{and} \quad \mathbf{W}^s = \mathbf{0}; \tag{2.9}$$

and since $\dot{J}^s = J^s \operatorname{tr} \mathbf{D}^s$, we have

$$\mathbf{D}^s = \frac{1}{3} (\dot{J}^s J^{s-1}) \mathbf{1}. \tag{2.10}$$

Finally, throughout we denote by P an arbitrary part of the reference body B with $\mathbf{n}_\mathrm{R}$ the outward unit normal on the boundary $\partial \mathrm{P}$ of P. Also, we denote by $\mathcal{P}_t = \boldsymbol{\chi}(\mathrm{P}, t)$ the image of P in the deformed body $\mathcal{B}_t = \boldsymbol{\chi}(\mathrm{B}, t)$, with $\mathbf{n}$ the outward unit normal on the boundary $\partial \mathcal{P}_t$ of $\mathcal{P}_t$.

2.2. Effective bond stretch

Following Mao et al. (2017b) we introduce a dimensionless positive-valued internal variable,

$$\lambda_b \in [1, \infty),$$

to represent (at the continuum scale) a measure of the stretch of the Kuhn segments of the polymer chains of the elastomeric gel. We call λ_b the effective bond stretch.

2.3. Damage variable

To describe damage and fracture of the gel we introduce an damage variable or phase-field,

$$d(\mathbf{X}, t) \in [0, 1]. \tag{2.11}$$

If $d = 0$ at a point then that point is intact, while if $d = 1$ at some point, then that point is fractured. Values of d between zero and one correspond to partially-fractured material. We assume that d grows monotonically so that

$$\dot{d}(\mathbf{X}, t) \geq 0, \tag{2.12}$$

which is a constraint that represents the usual assumption that microstructural changes leading to fracture are irreversible.

2.4. Fluid content. Balance law for the fluid content

Let

$$c_\mathrm{R}(\mathbf{X}, t) \tag{2.13}$$

denote the number of moles of fluid molecules absorbed by the elastomer, reckoned per unit volume of the dry elastomer. We call c_R the fluid content. The initial value of c_R in the wet elastomeric gel is denoted by $c_{\mathrm{R}0}$.

Define a fluid flux $\mathbf{j}_\mathrm{R}$, measured per unit area, per unit time, so that $-\int_{\partial \mathrm{P}} \mathbf{j}_\mathrm{R} \cdot \mathbf{n}_\mathrm{R} da_\mathrm{R}$ represents the number of moles of fluid entering P across $\partial \mathrm{P}$, per unit time. In this case the balance law for fluid content takes the form

$$\dot{\int_\mathrm{P} (c_\mathrm{R} - c_{\mathrm{R}0})\, dv_\mathrm{R}} = -\int_{\partial \mathrm{P}} \mathbf{j}_\mathrm{R} \cdot \mathbf{n}_\mathrm{R}\, da_\mathrm{R}, \tag{2.14}$$

for every part P. Bringing the time derivative in (2.14) inside the integral and using the divergence theorem on the integral over $\partial \mathrm{P}$, and localization the result leads to the following (local) balance law for the fluid content,

$$\dot{c}_\mathrm{R} = -\operatorname{Div} \mathbf{j}_\mathrm{R}. \tag{2.15}$$

2.5. Kinematical constitutive relation between J^s and c_R

Now, (J^s-1) represents the change in volume per unit reference volume due to swelling. We assume that this change arises entirely due to the change in the fluid content, so that with Ω denoting the volume of a mole of fluid molecules (presumed to be constant) we have the important swelling constraint,

$$J^s = 1 + \Omega\,(c_{\rm R} - c_{\rm R0}). \tag{2.16}$$

Note that on account of (2.8), the constraint (2.16) may also be stated as

$$\lambda^s = (1 + \Omega\,(c_{\rm R} - c_{\rm R0}))^{1/3}. \tag{2.17}$$

Finally, using (2.1) and (2.16) we may write $(2.6)_1$, for future use, as

$$(\nabla\dot{\boldsymbol{\chi}})\mathbf{F}^{-1} = \dot{\mathbf{F}}^e\mathbf{F}^{e-1} + \frac{1}{3}\Theta(c_{\rm R}, c_{\rm R0})\dot{c}_{\rm R}\mathbf{1}, \tag{2.18}$$

where

$$\Theta(c_{\rm R}, c_{\rm R0}) \stackrel{\rm def}{=} \frac{\Omega}{1+\Omega(c_{\rm R}-c_{\rm R0})} = J^{s-1}\Omega. \tag{2.19}$$

2.6. Principle of virtual power. Balance of forces

We follow Gurtin et al. (2010) and Anand (2012) to derive macroscopic and microscopic force balances via the principle of virtual power. In developing our theory we take the "rate-like" kinematical descriptors to be $\dot{\boldsymbol{\chi}}$, $\dot{\mathbf{F}}^e$, $\dot{c}_{\rm R}$, $\dot{\lambda}_b$, and $\dot{d}$, and also the gradient $\nabla\dot{d}$. In exploiting the principle of virtual power we note that the rates $(\dot{\boldsymbol{\chi}}, \dot{\mathbf{F}}^e, \dot{c}_{\rm R})$ are not independent-they are constrained by Eq. (2.18).

With each evolution of the body we associate macroscopic and microscopic force systems. The macroscopic system is defined by: (a) A traction $\mathbf{t}_{\rm R}(\mathbf{n}_{\rm R})$ that expends power over the velocity $\dot{\boldsymbol{\chi}}$. (b) A body force $\mathbf{b}_{\rm R}$ that also expends power over $\dot{\boldsymbol{\chi}}$. Regarding the body force, since time scales associated with the fluid diffusion are usually considerably longer than those associated with wave propagation, we neglect all inertial effects. (c) A stress $\mathbf{S}^e$ that expends power over the elastic distortion rate $\dot{\mathbf{F}}^e$.

The microscopic force system, which is non-standard, is defined by: (a) A scalar microscopic stress π that expend power over the rate $\dot{c}_{\rm R}$. (b) A scalar microscopic force f that expends power over the rate $\dot{\lambda}_b$. (c) A scalar microscopic stress ϖ that expends power over the rate $\dot{d}$. (d) A vector microscopic stress $\boldsymbol{\xi}$ that expends power over the gradient $\nabla\dot{d}$. (e) And a scalar microscopic traction $\xi\,(\mathbf{n}_{\rm R})$ that expends power over $\dot{d}$.

We characterize the force system through the manner in which these forces expend power. That is, given any part P, through the specification of $\mathcal{W}_{\rm ext}({\rm P})$, the power expended on P by material external to P, and $\mathcal{W}_{\rm int}({\rm P})$, a concomitant expenditure of power within P. Specifically,

$$\begin{aligned}
\mathcal{W}_{\rm ext}({\rm P}) &= \int_{\partial{\rm P}} \mathbf{t}_{\rm R}(\mathbf{n}_{\rm R})\cdot\dot{\boldsymbol{\chi}}\,{\rm d}a_{\rm R} + \int_{\rm P}\mathbf{b}_{\rm R}\cdot\dot{\boldsymbol{\chi}}\,{\rm d}v_{\rm R} + \int_{\partial{\rm P}}\xi\,(\mathbf{n}_{\rm R})\dot{d}\,{\rm d}a_{\rm R},\\
\mathcal{W}_{\rm int}({\rm P}) &= \int_{\rm P}\left(\mathbf{S}^e:\dot{\mathbf{F}}^e + \pi\dot{c}_{\rm R} + f\dot{\lambda}_b + \varpi\dot{d} + \boldsymbol{\xi}\cdot\nabla\dot{d}\right){\rm d}v_{\rm R},
\end{aligned} \tag{2.20}$$

where $\mathbf{S}^e, \pi, f, \varpi, \boldsymbol{\xi}$ are defined over the body for all time.

Assume that, at some arbitrarily chosen but *fixed time*, the fields $\boldsymbol{\chi}, \mathbf{F}, \mathbf{F}^e, c_{\rm R}, \lambda_b$, and d are known, and consider the fields $\dot{\boldsymbol{\chi}}, \dot{\mathbf{F}}^e, \dot{c}_{\rm R}, \dot{\lambda}_b$, and $\dot{d}$ are virtual velocities to be specified independently in a manner consistent with the constraint (2.18), i.e., denoting the virtual fields by $\tilde{\boldsymbol{\chi}}, \tilde{\mathbf{F}}^e, \tilde{c}_{\rm R}, \tilde{\lambda}_b$ and $\tilde{d}$ to differentiate them from fields asccociated with the actual evolution of the body, we require that

$$(\nabla\tilde{\boldsymbol{\chi}})\mathbf{F}^{-1} = \tilde{\mathbf{F}}^e\mathbf{F}^{e-1} + \frac{1}{3}\Theta(c_{\rm R}, c_{\rm R0})\tilde{c}_{\rm R}\mathbf{1}. \tag{2.21}$$

Further, we define a generalized virtual velocity to be a list

$$\mathcal{V} = (\tilde{\boldsymbol{\chi}}, \tilde{\mathbf{F}}^e, \tilde{c}_{\rm R}, \tilde{\lambda}_b, \tilde{d}), \tag{2.22}$$

consistent with (2.21). Also, we refer to a macroscopic virtual field $\mathcal{V}$ as rigid if it satisfies

$$(\nabla\tilde{\boldsymbol{\chi}}) = \tilde{\mathbf{F}} = \boldsymbol{\Omega}\mathbf{F} \qquad \text{together with} \qquad \tilde{\mathbf{F}} = \tilde{\mathbf{F}}^e, \qquad \tilde{c}_{\rm R} = 0, \qquad \tilde{\lambda}_b = 0, \qquad \tilde{d} = 0, \tag{2.23}$$

with $\boldsymbol{\Omega}$ a spatially constant skew tensor.

Writing

$$\mathcal{W}_{\text{ext}}(\mathrm{P}) = \int_{\partial \mathrm{P}} \mathbf{t}_{\mathrm{R}}(\mathbf{n}_{\mathrm{R}}) \cdot \tilde{\boldsymbol{\chi}} \mathrm{d}a_{\mathrm{R}} + \int_{\mathrm{P}} \mathbf{b}_{\mathrm{R}} \cdot \tilde{\boldsymbol{\chi}} \mathrm{d}v_{\mathrm{R}} + \int_{\partial \mathrm{P}} \xi(\mathbf{n}_{\mathrm{R}}) \tilde{d}\, da_{\mathrm{R}},$$
$$\mathcal{W}_{\text{int}}(\mathrm{P}) = \int_{\mathrm{P}} \left(\mathbf{S}^e : \tilde{\mathbf{F}}^e + \pi \tilde{c}_{\mathrm{R}} + f \tilde{\lambda}_b + \varpi \tilde{d} + \boldsymbol{\xi} \cdot \nabla \tilde{d} \right) \mathrm{d}v_{\mathrm{R}}, \tag{2.24}$$

respectively, for the external and internal expenditures of virtual power, the principle of virtual power consists of two basic requirements:

(V1) Given any part P,

$$\mathcal{W}_{\text{ext}}(\mathrm{P}, \mathcal{V}) = \mathcal{W}_{\text{int}}(\mathrm{P}, \mathcal{V}) \quad \text{for all generalized virtual velocities } \mathcal{V}. \tag{2.25}$$

(V2) Given any part P and a rigid virtual velocity $\mathcal{V}$,

$$\mathcal{W}_{\text{int}}(\mathrm{P}, \mathcal{V}) = 0 \text{ whenever } \mathcal{V} \text{ is a rigid macroscopic virtual velocity.} \tag{2.26}$$

2.6.1. Consequences of the principle of virtual power

The virtual-power principle has the following consequences:

(a) The stress

$$\mathbf{T}_{\mathrm{R}} \stackrel{\text{def}}{=} \mathbf{S}^e \mathbf{F}^{s-\top}, \tag{2.27}$$

is consistent with a macroscopic force balance and a macroscopic traction condition,

$$\mathrm{Div}\, \mathbf{T}_{\mathrm{R}} + \mathbf{b}_{\mathrm{R}} = \mathbf{0} \qquad \text{and} \qquad \mathbf{t}_{\mathrm{R}}(\mathbf{n}_{\mathrm{R}}) = \mathbf{T}_{\mathrm{R}} \mathbf{n}_{\mathrm{R}}, \tag{2.28}$$

and $\mathbf{T}_{\mathrm{R}} \mathbf{F}^{\top}$ is symmetric,

$$\mathbf{T}_{\mathrm{R}} \mathbf{F}^{\top} = \mathbf{F} \mathbf{T}_{\mathrm{R}}^{\top}. \tag{2.29}$$

In view of (2.28) and (2.29) the stress $\mathbf{T}_{\mathrm{R}}$ represents the classical Piola stress, with (2.28) and (2.29) representing the local macroscopic force and moment balances in the reference body.

As is standard, the Piola stress $\mathbf{T}_{\mathrm{R}}$ is related to the symmetric Cauchy stress $\mathbf{T}$ in the deformed body by

$$\mathbf{T}_{\mathrm{R}} = J \mathbf{T} \mathbf{F}^{-\top}, \tag{2.30}$$

so that

$$\mathbf{T} = J^{-1} \mathbf{T}_{\mathrm{R}} \mathbf{F}^{\top}. \tag{2.31}$$

It is convenient to introduce two new stress measures:

- The elastic second Piola stress,

$$\mathbf{T}^e \stackrel{\text{def}}{=} J^e \mathbf{F}^{e-1} \mathbf{T} \mathbf{F}^{e-\top}, \tag{2.32}$$

  which is symmetric on account of the symmetry of the Cauchy stress $\mathbf{T}$.
- The Mandel stress,

$$\mathbf{M}^e \stackrel{\text{def}}{=} \mathbf{C}^e \mathbf{T}^e = J^e \mathbf{F}^{e\top} \mathbf{T} \mathbf{F}^{e-\top}, \tag{2.33}$$

  which in general is not symmetric.

Using (2.27), (2.30), and (2.2) we find that

$$\mathbf{S}^e = J \mathbf{T} \mathbf{F}^{e-\top}. \tag{2.34}$$

Thus, using the definitions (2.32) and (2.33) we find that

$$\mathbf{F}^{e-1} \mathbf{S}^e = J^s \mathbf{T}^e, \quad \text{and} \quad \mathbf{F}^{e\top} \mathbf{S}^e = J^s \mathbf{M}^e. \tag{2.35}$$

(b) The microscopic force balance

$$\pi = \frac{1}{3} \Theta(c_{\mathrm{R}}, c_{\mathrm{R}0}) J^s \mathrm{tr} \mathbf{M}^{\mathrm{e}} = \Omega \left(\frac{1}{3} \mathrm{tr} \mathbf{M}^{\mathrm{e}} \right), \tag{2.36}$$

where in writing the last of (2.36) we have used (2.19).

(c) The microstresses $\boldsymbol{\xi}$ and ϖ are consistent with the microforce balance and microtraction condition,

$$\mathrm{Div}\, \boldsymbol{\xi} - \varpi = 0, \qquad \text{and} \qquad \xi(\mathbf{n}_{\mathrm{R}}) = \boldsymbol{\xi} \cdot \mathbf{n}_{\mathrm{R}}. \tag{2.37}$$

(d) The microscopic force f which is conjugate to $\dot{\lambda}_b$ satisfies,

$$f = 0. \tag{2.38}$$

The requirement that $f = 0$ implies that a variation of λ_b expends no internal power. At first blush it appears that the "microforce balance" (2.38) is devoid of physical content. However, it does have physical content, which is revealed later when we consider our thermodynamically consistent constitutive theory. As we shall see (2.38) will imply an internal constraint equation between λ_b and the right Cauchy-Green tensor $\mathbf{C}$ and other constitutive variables of the form $f(\mathbf{C}^e, c_{\mathrm{R}}, \lambda_b, d, \nabla d) = 0$, which will serve as an implicit equation for determining λ_b in terms of the other constitutive variables.

Finally, using the traction conditions $(2.28)_2$ and $(2.37)_2$, the actual external expenditure of power is

$$\mathcal{W}_{\text{ext}}(\mathrm{P}) = \int_{\partial \mathrm{P}} (\mathbf{T}_{\mathrm{R}}\mathbf{n}_{\mathrm{R}}) \cdot \dot{\boldsymbol{\chi}}\, da_{\mathrm{R}} + \int_{\mathrm{P}} \mathbf{b}_{\mathrm{R}} \cdot \dot{\boldsymbol{\chi}}\, dv_{\mathrm{R}} + \int_{\partial \mathrm{P}} (\boldsymbol{\xi} \cdot \mathbf{n}_{\mathrm{R}}) \dot{d}\, da_{\mathrm{R}}. \tag{2.39}$$

Also, using $(2.35)_1$ and $(2.5)_2$ the stress power $\mathbf{S}^e : \dot{\mathbf{F}}^e$ may be alternatively written as

$$\mathbf{S}^e : \dot{\mathbf{F}}^e = (J^s\mathbf{T}^e) : (\mathbf{F}^{e\top}\dot{\mathbf{F}}^e) = \tfrac{1}{2}(J^s\mathbf{T}^e) : \dot{\mathbf{C}}^e. \tag{2.40}$$

Thus the corresponding internal expenditure of power may be written as

$$\mathcal{W}_{\text{int}}(\mathrm{P}) = \int_{\mathrm{P}} \Big(\frac{1}{2}(J^s\mathbf{T}^e) : \dot{\mathbf{C}}^e + \pi \dot{c}_{\mathrm{R}} + f\dot{\lambda}_b + \varpi \dot{d} + \boldsymbol{\xi} \cdot \nabla d \Big) \mathrm{d}v_{\mathrm{R}}. \tag{2.41}$$

2.7. Free energy imbalance

Our discussion of thermodynamics involves the following fields: (i) ε_{R}, the internal energy density per unit reference volume; (ii) η_{R}, the entropy density per unit reference volume; (iii) $\mathbf{q}_{\mathrm{R}}$, the heat flux per unit reference area; (iv) q_{R}, the external heat supply per unit reference volume; (v) ϑ, the absolute temperature ($\vartheta > 0$); (vi) μ_{R}, the chemical potential, and follows the discussion of Gurtin (1996) and Gurtin et al. (2010, Section 64).

Consider a material region P. Then, consistent with our omission of inertial effects, we neglect kinetic energy, and take the balance law for energy as,

$$\dot{\int_{\mathrm{P}} \varepsilon_{\mathrm{R}}\, dv_{\mathrm{R}}} = -\int_{\partial \mathrm{P}} \mathbf{q}_{\mathrm{R}} \cdot \mathbf{n}_{\mathrm{R}}\, da_{\mathrm{R}} + \int_{\mathrm{P}} q_{\mathrm{R}}\, dv_{\mathrm{R}} + \mathcal{W}_{\text{ext}}(\mathrm{P}) - \int_{\partial \mathrm{P}} \mu_{\mathrm{R}} \mathbf{j}_{\mathrm{R}} \cdot \mathbf{n}_{\mathrm{R}} da_{\mathrm{R}}, \tag{2.42}$$

where the last term in (2.42) represents the flux of energy carried into P by the flux $\mathbf{j}_{\mathrm{R}}$ of the diffusing fluid. Also, the second law takes the form of an entropy imbalance

$$\dot{\int_{\mathrm{P}} \eta_{\mathrm{R}}\, dv_{\mathrm{R}}} \geq -\int_{\partial \mathrm{P}} \frac{\mathbf{q}_{\mathrm{R}} \cdot \mathbf{n}_{\mathrm{R}}}{\vartheta}\, da_{\mathrm{R}} + \int_{\mathrm{P}} \frac{q_{\mathrm{R}}}{\vartheta}\, dv_{\mathrm{R}}. \tag{2.43}$$

Assume now that isothermal conditions prevail, so that $\vartheta \equiv$ constant, and introduce the Helmholtz free energy per unit reference volume defined by $\psi_{\mathrm{R}} = \varepsilon_{\mathrm{R}} - \vartheta \eta_{\mathrm{R}}$. Then, upon multiplying the entropy imbalance (2.43) by ϑ and subtracting the result from the energy balance (2.42) yields the free energy imbalance

$$\dot{\int_{\mathrm{P}} \psi_{\mathrm{R}}\, dv_{\mathrm{R}}} \leq \mathcal{W}_{\text{ext}}(\mathrm{P}) - \int_{\partial \mathrm{P}} \mu_{\mathrm{R}} \mathbf{j}_{\mathrm{R}} \cdot \mathbf{n}_{\mathrm{R}} da_{\mathrm{R}}. \tag{2.44}$$

We henceforth restrict attention to isothermal processes and for that reason base the theory on the free energy imbalance (2.44).

Thus, since $\mathcal{W}_{\text{ext}}(\mathrm{P}) = \mathcal{W}_{\text{int}}(\mathrm{P})$, upon recalling (2.41) and applying the divergence theorem to the term in (2.44) involving an integral over the boundary ∂P of P, use of the balance law (2.15), and localizing the expression gives the following local form of the free energy imbalance,

$$\dot{\psi}_{\mathrm{R}} - \tfrac{1}{2}(J^s\mathbf{T}^e) : \dot{\mathbf{C}}^e - \mu_{\mathrm{R}}^{\text{net}} \dot{c}_{\mathrm{R}} - f\dot{\lambda}_b - \varpi \dot{d} - \boldsymbol{\xi} \cdot \nabla \dot{d} + \mathbf{j}_{\mathrm{R}} \cdot \nabla \mu_{\mathrm{R}} \leq 0\,, \tag{2.45}$$

where we have written

$$\mu_{\mathrm{R}}^{\text{net}} \stackrel{\text{def}}{=} \mu_{\mathrm{R}} + \pi \tag{2.46}$$

for a net chemical potential.

For later use we define the dissipation density $\mathcal{D} \geq 0$ per unit volume per unit time by,

$$\mathcal{D} = \tfrac{1}{2}(J^s\mathbf{T}^e) : \dot{\mathbf{C}}^e + \mu_{\mathrm{R}}^{\text{net}} \dot{c}_{\mathrm{R}} + f\dot{\lambda}_b + \varpi \dot{d} + \boldsymbol{\xi} \cdot \nabla \dot{d} - \mathbf{j}_{\mathrm{R}} \cdot \nabla \mu_{\mathrm{R}} - \dot{\psi}_{\mathrm{R}} \geq 0. \tag{2.47}$$

Remark. For brevity we have not discussed the transformation properties under a change in frame of the various fields appearing in our theory. Here, we simply note that all quantities in the free energy imbalance (2.45) are invariant under a change in frame (Gurtin et al., 2010).

2.8. Constitutive theory

Let $\boldsymbol{\Lambda}$ represent the list

$$\boldsymbol{\Lambda} = \{\mathbf{C}^e, c_{\mathrm{R}}, \lambda_b\,, d, \nabla d\}. \tag{2.48}$$

Guided by (2.45), we beginning by assuming constitutive equations for the free energy ψ_{R}, the stress $\mathbf{T}^e$, the net chemical potential $\mu_{\mathrm{R}}^{\text{net}}$, the scalar microstresses f and ϖ, and the vector microstress $\boldsymbol{\xi}$ are given by the constitutive equations

$$\psi_{\mathrm{R}} = \hat{\psi}_{\mathrm{R}}(\boldsymbol{\Lambda}), \qquad \mathbf{T}^e = \hat{\mathbf{T}}^e(\boldsymbol{\Lambda}), \qquad \mu_{\mathrm{R}}^{\text{net}} = \hat{\mu}_{\mathrm{R}}^{\text{net}}(\boldsymbol{\Lambda}), \quad f = \hat{f}(\boldsymbol{\Lambda}), \qquad \varpi = \hat{\varpi}(\boldsymbol{\Lambda}), \qquad \boldsymbol{\xi} = \hat{\boldsymbol{\xi}}(\boldsymbol{\Lambda}). \tag{2.49}$$

Then,

$$\dot{\psi}_{\rm R} = \frac{\partial \hat{\psi}_{\rm R}(\mathbf{\Lambda})}{\partial \mathbf{C}^e} : \dot{\mathbf{C}}^e + \frac{\partial \hat{\psi}_{\rm R}(\mathbf{\Lambda})}{\partial c_{\rm R}} \dot{c}_{\rm R} + \frac{\partial \hat{\psi}_{\rm R}(\mathbf{\Lambda})}{\partial \lambda_b} \dot{\lambda}_b + \frac{\partial \hat{\psi}_{\rm R}(\mathbf{\Lambda})}{\partial d} \dot{d} + \frac{\partial \hat{\psi}_{\rm R}(\mathbf{\Lambda})}{\partial \nabla d} \cdot \nabla \dot{d}. \tag{2.50}$$

Using (2.50) and substituting the constitutive equations (2.49) into the free-energy imbalance (2.45), we find that it may then be written as

$$\begin{aligned} &\left[\frac{\partial \hat{\psi}_{\rm R}(\mathbf{\Lambda})}{\partial \mathbf{C}^e} - \tfrac{1}{2} J^s \hat{\mathbf{T}}^e(\mathbf{\Lambda}) \right] : \dot{\mathbf{C}}^e + \left[\frac{\partial \hat{\psi}_{\rm R}(\mathbf{\Lambda})}{\partial c_{\rm R}} - \hat{\mu}_{\rm R}^{\rm net}(\mathbf{\Lambda}) \right] \dot{c}_{\rm R} \\ &\qquad + \left[\frac{\partial \hat{\psi}_{\rm R}(\mathbf{\Lambda})}{\partial \lambda_b} - \hat{f}(\mathbf{\Lambda}) \right] \dot{\lambda}_b + \left[\frac{\partial \hat{\psi}_{\rm R}(\mathbf{\Lambda})}{\partial d} - \varpi \right] \dot{d} + \left[\frac{\partial \hat{\psi}_{\rm R}(\mathbf{\Lambda})}{\partial \nabla d} - \boldsymbol{\xi} \right] \cdot \nabla \dot{d} + \mathbf{j}_{\rm R} \cdot \nabla \mu_{\rm R} \leq 0. \end{aligned} \tag{2.51}$$

We assume, constitutively, that the free-energy delivers the stress $\mathbf{T}^e$ and the net chemical potential through the state relations

$$\mathbf{T}^e = 2J^{s-1} \frac{\partial \hat{\psi}_{\rm R}(\mathbf{\Lambda})}{\partial \mathbf{C}^e}, \qquad \text{and} \qquad \mu_{\rm R}^{\rm net} = \frac{\partial \hat{\psi}_{\rm R}(\mathbf{\Lambda})}{\partial c_{\rm R}}. \tag{2.52}$$

Further, we introduce an energetic microforce $f_{\rm en}$, and energetic microstresses $\varpi_{\rm en}$ and $\boldsymbol{\xi}_{\rm en}$ through

$$f_{\rm en} \stackrel{\rm def}{=} \frac{\partial \hat{\psi}_{\rm R}(\mathbf{\Lambda})}{\partial \lambda_b}, \qquad \varpi_{\rm en} \stackrel{\rm def}{=} \frac{\partial \hat{\psi}_{\rm R}(\mathbf{\Lambda})}{\partial d}, \qquad \boldsymbol{\xi}_{\rm en} \stackrel{\rm def}{=} \frac{\partial \hat{\psi}_{\rm R}(\mathbf{\Lambda})}{\partial \nabla d}, \tag{2.53}$$

respectively, and guided by (2.51) also introduce a dissipative microforce $f_{\rm diss}$, and dissipative microstresses $\varpi_{\rm diss}$ and $\boldsymbol{\xi}_{\rm diss}$ through

$$f_{\rm diss} \stackrel{\rm def}{=} f - f_{\rm en}, \qquad \varpi_{\rm diss} \stackrel{\rm def}{=} \varpi - \varpi_{\rm en}, \qquad \boldsymbol{\xi}_{\rm diss} \stackrel{\rm def}{=} \boldsymbol{\xi} - \boldsymbol{\xi}_{\rm en}. \tag{2.54}$$

Using (2.52), (2.53) and (2.54), leads to the following reduced dissipation inequality

$$\mathcal{D} = f_{\rm diss} \dot{\lambda}_b + \varpi_{\rm diss} \dot{d} + \boldsymbol{\xi}_{\rm diss} \cdot \nabla \dot{d} - \mathbf{j}_{\rm R} \cdot \nabla \mu_{\rm R} \geq 0. \tag{2.55}$$

Next, we assume that the vector microstress $\boldsymbol{\xi}$ is purely energetic so that

$$\boldsymbol{\xi}_{\rm diss} = \mathbf{0}. \tag{2.56}$$

Further, in order to satisfy (2.55) we assume that each of the terms separately satisfy dissipation inequalities of the form,

$$\begin{aligned} &f_{\rm diss} \dot{\lambda}_b > 0 \quad \text{for} \quad \dot{\lambda}_b > 0, \\ &\varpi_{\rm diss} \dot{d} > 0 \quad \text{for} \quad \dot{d} > 0, \\ &-\mathbf{j}_{\rm R} \cdot \nabla \mu_{\rm R} > 0 \quad \text{for} \quad \nabla \mu_{\rm R} \neq \mathbf{0}. \end{aligned} \tag{2.57}$$

Next, we assume that $\varpi_{\rm diss}$ is given by

$$\varpi_{\rm diss} = \alpha + \zeta \dot{d}, \qquad \text{with} \qquad \alpha = \hat{\alpha}(\mathbf{\Lambda}) > 0 \quad \text{and} \quad \zeta = \hat{\zeta}_{\rm dam}(\mathbf{\Lambda}) > 0, \tag{2.58}$$

so that the dissipation inequality $(2.57)_1$ is satisfied, in the sense that

$$\left(\alpha + \zeta \dot{d}\right) \dot{d} > 0 \quad \text{whenever} \quad \dot{d} > 0. \tag{2.59}$$

Further, we assume that $f_{\rm diss}$ is given by

$$f_{\rm diss} = \kappa_b \dot{\lambda}_b, \qquad \text{with} \qquad \kappa_b = \hat{\kappa}_b(\mathbf{\Lambda}) > 0, \tag{2.60}$$

so that the dissipation inequality $(2.57)_2$ is satisfied, in the sense that

$$\left(\kappa_b \dot{\lambda}_b\right) \dot{\lambda}_b > 0 \quad \text{whenever} \quad \dot{\lambda}_b > 0. \tag{2.61}$$

Thus summarizing, from the equations above we have the following thermodynamically-consistent constitutive equations for the microforce f and the microstresses ϖ and $\boldsymbol{\xi}$:

$$f = \frac{\partial \hat{\psi}_{\rm R}(\mathbf{\Lambda})}{\partial \lambda_b} + \hat{\kappa}_b(\mathbf{\Lambda}) \dot{\lambda}_b, \qquad \varpi = \frac{\partial \hat{\psi}_{\rm R}(\mathbf{\Lambda})}{\partial d} + \hat{\alpha}(\mathbf{\Lambda}) + \hat{\zeta}(\mathbf{\Lambda}) \dot{d}, \qquad \boldsymbol{\xi} = \frac{\partial \hat{\psi}_{\rm R}(\mathbf{\Lambda})}{\partial \nabla d}. \tag{2.62}$$

Finally, we assume that the fluid flux $\mathbf{j}_{\rm R}$ obeys a Fick-type relation in the sense that the fluid flux $\mathbf{j}_{\rm R}$ depends linearly on the gradient of the chemical potential,

$$\mathbf{j}_{\rm R} = -\mathbf{M}(\mathbf{\Lambda}) \nabla \mu_{\rm R}, \tag{2.63}$$

where $\mathbf{M}$ is a mobility tensor. Note that on account of $(2.57)_2$, the mobility tensor is positive definite.

2.9. Chemical potential

The microforce balance (2.36), when combined with the thermodynamically consistent constitutive equation $(2.52)_2$, together with the definition (2.46) of $\mu_{\mathrm{R}}^{\mathrm{net}}$, gives the following important expression for the chemical potential in the theory,

$$\mu_{\mathrm{R}} = \frac{\partial \hat{\psi}_{\mathrm{R}}(\boldsymbol{\Lambda})}{\partial c_{\mathrm{R}}} - \Omega\big(\frac{1}{3}\mathrm{tr}\mathbf{M}^{\mathrm{e}}\big)\,. \tag{2.64}$$

2.10. Evolution equation for the bond stretch

The microforce balance (2.38), viz.

$$f = 0, \tag{2.65}$$

together with the constitutive equation $(2.62)_1$ gives the important thermodynamically-consistent Ginzburg–Landau-type equation,

$$\hat{\kappa}_b(\boldsymbol{\Lambda})\,\dot{\lambda}_b = -\frac{\partial \hat{\psi}_{\mathrm{R}}(\boldsymbol{\Lambda})}{\partial \lambda_b}, \tag{2.66}$$

which serves as an evolution equation for λ_b.

2.11. Evolution equation for the damage variable

The microforce balance (2.37), viz.

$$\mathrm{Div}\,\boldsymbol{\xi} - \varpi = 0, \tag{2.67}$$

together with the constitutive equations $(2.62)_{2,\,3}$ gives the evolution equation for the damage variable d as

$$\hat{\zeta}(\boldsymbol{\Lambda})\dot{d} = F(\boldsymbol{\Lambda}) \qquad \text{for} \qquad \dot{d} > 0, \qquad \text{where} \qquad F(\boldsymbol{\Lambda}) \stackrel{\text{def}}{=} \left[-\frac{\partial \hat{\psi}_{\mathrm{R}}(\boldsymbol{\Lambda})}{\partial d} + \mathrm{Div}\left(\frac{\partial \hat{\psi}_{\mathrm{R}}(\boldsymbol{\Lambda})}{\partial \nabla d}\right)\right] - \hat{\alpha}(\boldsymbol{\Lambda}). \tag{2.68}$$

Since ζ is positive-valued, F must be positive for $\dot{d}$ to be positive, and the damage to increase.

2.12. Boundary and initial conditions

We also need boundary and initial conditions to complete the theory.

1. **Boundary conditions for the partial differential equation (pde) governing the evolution of the motion $\boldsymbol{\chi}$:**
   Let $\mathcal{S}_{\boldsymbol{\chi}}$ and $\mathcal{S}_{\mathbf{t}_{\mathrm{R}}}$ be complementary subsurfaces of the boundary $\partial\mathrm{B}$ of the body B. Then for a time interval $t \in [0,\,T]$ we consider a pair of boundary conditions in which the motion is specified on $\mathcal{S}_{\boldsymbol{\chi}}$ and the surface traction on $\mathcal{S}_{\mathbf{t}_{\mathrm{R}}}$:
   $$\boldsymbol{\chi} = \check{\boldsymbol{\chi}} \quad \text{on } \mathcal{S}_{\boldsymbol{\chi}} \times [0,T], \qquad \text{and} \qquad \mathbf{T}_{\mathrm{R}}\mathbf{n}_{\mathrm{R}} = \check{\mathbf{t}}_{\mathrm{R}} \qquad \text{on } \mathcal{S}_{\mathbf{t}_{\mathrm{R}}} \times [0,T], \tag{2.69}$$
   where $\check{\boldsymbol{\chi}}$ and $\check{\mathbf{t}}_{\mathrm{R}}$ are prescribed functions of $\mathbf{X}$ and t.
2. **Boundary conditions for the pde governing the evolution of μ_{R}:**
   Using (2.63) and (2.64) the balance equation (2.15) for c_{R} may be stated as a balance equation for the chemical potential μ_{R}. Let $\mathcal{S}_{\mu_{\mathrm{R}}}$ and $\mathcal{S}_{\mathbf{j}_{\mathrm{R}}}$ be complementary subsurfaces of the boundary $\partial\mathrm{B}$ of the body B. Then for a time interval $t \in [0,\,T]$ we consider a pair of boundary conditions in which the chemical potential is specified on $\mathcal{S}_{\mu_{\mathrm{R}}}$ and the fluid flux on $\mathcal{S}_{\mathbf{j}_{\mathrm{R}}}$:
   $$\mu_{\mathrm{R}} = \check{\mu}_{\mathrm{R}} \quad \text{on } \mathcal{S}_{\mu_{\mathrm{R}}} \times [0,T], \qquad \text{and} \qquad \mathbf{j}_{\mathrm{R}} \cdot \mathbf{n}_{\mathrm{R}} = \check{j}_{\mathrm{R}} \qquad \text{on } \mathcal{S}_{\mathbf{j}_{\mathrm{R}}} \times [0,T], \tag{2.70}$$
   where $\check{\mu}_{\mathrm{R}}$ and $\check{j}_{\mathrm{R}}$ are prescribed functions of $\mathbf{X}$ and t.
3. **Boundary conditions for the pde governing the evolution of d:**
   The presence of microscopic stresses $\boldsymbol{\xi}$ results in an expenditure of power
   $$\int_{\partial\mathrm{B}} (\boldsymbol{\xi}\cdot\mathbf{n}_{\mathrm{R}})\dot{d}\;\mathrm{d}a_{\mathrm{R}}$$
   by the material in contact with the body, and this necessitates a consideration of boundary conditions on $\partial\mathrm{B}$ involving the microscopic tractions $\boldsymbol{\xi}\cdot\mathbf{n}_{\mathrm{R}}$ and the rate of change of the damage variable $\dot{d}$.
   - We restrict attention to the simplest set of boundary conditions that result in a null expenditure of microscopic power in the sense that $(\boldsymbol{\xi}\cdot\mathbf{n}_{\mathrm{R}})\dot{d} = 0$.

   A set of boundary conditions which satisfies this requirement is,
   $$\dot{d} = 0 \quad \text{on } \mathcal{S}_d \times [0,T], \qquad \text{and} \qquad \boldsymbol{\xi}\cdot\mathbf{n}_{\mathrm{R}} = 0 \quad \text{on } \partial\ \mathrm{B} \setminus \mathcal{S}_d \times [0,T], \tag{2.71}$$
   with the microforce $\boldsymbol{\xi}$ given by $(2.62)_3$.

The initial conditions for the motion, chemical potential, and damage are taken as,

$$\boldsymbol{\chi}(\mathbf{X},0) = \mathbf{X}, \quad \mu_{\mathrm{R}}(\mathbf{X},0) = \mu_{\mathrm{R}0}(\mathbf{X}) \quad \text{and} \quad d(\mathbf{X},0) = 0. \quad \text{in} \quad \mathrm{B}. \tag{2.72}$$

3. Specialization of the constitutive equations

3.1. Specialized form for the free energy ψ_R

3.1.1. Specialized form for the free energy with no bond stretch and no damage

We begin by recalling a set of specialized equations proposed by Chester and Anand for an elastomeric gel in which there are no energetic effects due to bond-stretch and there is no damage (Chester and Anand, 2010; 2011). Limiting our considerations to isotropic materials under isothermal conditions, we begin by assuming that the free energy ψ_{R} may be written in a separable form as

$$\tilde{\psi}_{\mathrm{R}}(\mathcal{I}_{\mathbf{C}^e}, c_{\mathrm{R}}, \vartheta) = \mu_{\mathrm{R}}^0 c_{\mathrm{R}} + \psi_{\mathrm{R}}^{\mathrm{mix}}(c_{\mathrm{R}}, \vartheta) + \psi_{\mathrm{R}}^{\mathrm{mech}}(\mathcal{I}_{\mathbf{C}^e}, c_{\mathrm{R}}, \vartheta), \tag{3.1}$$

where $\mathcal{I}_{\mathbf{C}^e}$ are the principal invariants of $\mathbf{C}^e$, μ_{R}^0 is the chemical potential of the unmixed pure solvent, $\psi_{\mathrm{R}}^{\mathrm{mix}}(c_{\mathrm{R}}, \vartheta)$ is the change in free energy due to mixing of the solvent with the polymer network, $\psi_{\mathrm{R}}^{\mathrm{mech}}(\mathcal{I}_{\mathbf{C}^e}, c_{\mathrm{R}}, \vartheta)$ is the contribution to the change in the free energy due to the deformation of the polymer network.

Polymer volume fraction

In the literature on swelling of elastomers, the quantity

$$\phi \stackrel{\mathrm{def}}{=} \frac{1 - \Omega c_{\mathrm{R0}}}{1 + \Omega\,(c_{\mathrm{R}} - c_{\mathrm{R0}})} = (1 - \Omega c_{\mathrm{R0}})(\lambda^s)^{-3} = (1 - \Omega c_{\mathrm{R0}})J^{s-1}, \tag{3.2}$$

is called the polymer volume fraction, with $\phi_0 \stackrel{\mathrm{def}}{=} 1 - \Omega c_{\mathrm{R0}}$ the initial volume fraction of the polymer. If the elastomer is dry, that is $c_{\mathrm{R0}} = 0$, then $\phi_0 = 1$.[4]

Estimate for ψ_R^{mix}

Next, we adopt the following classical from of the theory for the contribution to the free energy due to mixing (Flory, 1942; Flory and Rehner, 1943; Huggins, 1942),

$$\psi_{\mathrm{R}}^{\mathrm{mix}} = \frac{R\vartheta}{\Omega}\left[\frac{\phi_0}{\phi}\Big((1-\phi)\ln(1-\phi) + \chi\phi(1-\phi)\Big)\right], \tag{3.3}$$

where R is the universal gas constant, and χ is a dimensionless parameter (called the χ-parameter, or Flory-Huggins interaction parameter), which represents the dis-affinity between the polymer and the fluid:

- a low value of χ favors swelling, while a high value of χ favours de-swelling.

Estimate for ψ_R^{mech}

In elastomeric materials, the major part of $\psi_{\mathrm{R}}^{\mathrm{mech}}$ arises from an entropic contribution. Let

$$\bar{\lambda} \stackrel{\mathrm{def}}{=} \frac{1}{\sqrt{3}}\sqrt{\mathrm{tr}\mathbf{C}} = \frac{1}{\sqrt{3}}\sqrt{(\mathrm{tr}\mathbf{C}^{\mathrm{e}})(1 + \Omega\,(c_{\mathrm{R}} - c_{\mathrm{R0}}))^{2/3}} \tag{3.4}$$

define an effective total stretch. If we introduce an effective elastic stretch by

$$\bar{\lambda}^e \stackrel{\mathrm{def}}{=} \frac{1}{\sqrt{3}}\sqrt{\mathrm{tr}\mathbf{C}^{\mathrm{e}}}, \tag{3.5}$$

then recalling (2.17), the effective total stretch is given by the product of the swelling stretch and the effective elastic stretch,

$$\bar{\lambda} = \bar{\lambda}^e\lambda^s. \tag{3.6}$$

The classical statistical-mechanical models of rubber elasticity which use non-Gaussian statistics to account for the limited extensibility of the polymer chains, provide the following estimates for the entropy change due to mechanical stretching (cf., e.g., Arruda and Boyce, 1993; Treloar, 1975),

$$\eta_{\mathrm{R}}^{\mathrm{mech}} = -Nk_Bn\left[\left(\frac{\bar{\lambda}}{\sqrt{n}}\right)\beta + \ln\left(\frac{\beta}{\sinh\beta}\right)\right] + Nk_B\left(\frac{\sqrt{n}}{3}\beta_0\right)\ln J, \tag{3.7}$$

with k_B Boltzmann's constant,

$$\beta \stackrel{\mathrm{def}}{=} \mathcal{L}^{-1}\left(\frac{\bar{\lambda}}{\sqrt{n}}\right), \qquad \text{and} \qquad \beta_0 \stackrel{\mathrm{def}}{=} \mathcal{L}^{-1}\left(\frac{1}{\sqrt{n}}\right), \tag{3.8}$$

[4] Note that while c_{R} is positive, it has no upper bound. However, the polymer volume fraction is constrained to lie in the range $\phi \in [0, 1]$; this is a useful feature of ϕ in numerical computations.

where $\mathcal{L}^{-1}$ is the inverse of the Langevin function $\mathcal{L}(x) = \coth(x) - (x)^{-1}$. This functional form for the change in entropy involves two material parameters: (i) N, the number of polymer chains per unit reference volume, and (ii) n the number of links in a freely-jointed chain.

To account for the interaction between the polymer chains and to account for a slight compressibility of the gel, Chester and Anand (2011) also introduced an energetic component,

$$\varepsilon_{\text{Rvol}} = \hat{\varepsilon}_{\text{Rvol}}(J^e), \tag{3.9}$$

to the free energy.

Then, using (3.7), (3.7), and (3.9), we obtain the estimate

$$\psi_{\text{R}}^{\text{mech}}(\mathcal{I}_{\mathbf{C}^e}, c_{\text{R}}, \vartheta) = (Nk_B\vartheta)\, n\left[\left(\frac{\bar{\lambda}}{\sqrt{n}}\right)\beta + \ln\left(\frac{\beta}{\sinh\beta}\right)\right] - (Nk_B\vartheta)\left(\frac{\sqrt{n}}{3}\beta_0\right)\ln J + \hat{\varepsilon}_{\text{Rvol}}(J^e), \tag{3.10}$$

with $\bar{\lambda}$ defined in (3.4).

Thus, using (3.3) and (3.10) in (3.1), a particular form of the free energy function which accounts for the combined effects of mixing, swelling, and elastic stretching proposed by Chester and Anand (2010, 2011) is

$$\begin{aligned}\psi_{\text{R}} = \mu_{\text{R}}^0 c_{\text{R}} + \frac{R\vartheta}{\Omega}\left[\frac{\phi_0}{\phi}\Big((1-\phi)\ln(1-\phi) + \chi\phi(1-\phi)\Big)\right] \\ + (Nk_B\vartheta)\, n\left[\left(\frac{\bar{\lambda}}{\sqrt{n}}\right)\beta + \ln\left(\frac{\beta}{\sinh\beta}\right)\right] - (Nk_B\vartheta)\left(\frac{\sqrt{n}}{3}\beta_0\right)\ln J + \hat{\varepsilon}_{\text{Rvol}}(J^e).\end{aligned} \tag{3.11}$$

3.1.2. Specialized form for the free energy accounting for bond stretch

In a recent paper Mao et al. (2017b) proposed a model for both deformation and fracture of elastomeric materials; their model is consistent with Arruda–Boyce model for deformation of elastomers (Arruda and Boyce, 1993), and the Lake–Thomas proposal for fracture of elastomers due to the scission of the Kuhn segments of polymer chains (Lake and Thomas, 1967).

Consider a single polymer chain. The essential idea in the paper by Mao et al. (2017b) is to assume that the Kuhn segments in a polymer chain are not rigid but is stretchable. Thus, let

λ_b denote the stretch of a Kuhn segment,

and for simplicity assume that each Kuhn segment in a chain stretches by the same amount. Every stretchable Kuhn segment can store an internal energy, which we denote by

$$\varepsilon_b = \hat{\varepsilon}_b(\lambda_b). \tag{3.12}$$

Under this assumption the change in entropy η of a chain has the same form as given by the classical inverse-Langevin formula, but instead of a constant Kuhn segment length L, the Kuhn segment length is

$$l = \lambda_b L,$$

and the expression for the change in entropy of a single chain according to the Langevin statistics becomes,

$$\eta = -n\,k_B\left[\left(\frac{\lambda\lambda_b^{-1}}{\sqrt{n}}\right)\beta + \ln\left(\frac{\beta}{\sinh\beta}\right)\right] \qquad \text{with} \qquad \beta = \mathcal{L}^{-1}\left(\frac{\lambda\lambda_b{}^{-1}}{\sqrt{n}}\right), \tag{3.13}$$

where n is the number of Kuhn segments in a chain, and where λ is the overall stretch of the polymer chain. Using (3.12) and (3.13), the free energy a single chain with stretchable Kuhn segments is then given by

$$\psi = n\hat{\varepsilon}_b(\lambda_b) + nk_B\vartheta\left[\left(\frac{\lambda\lambda_b^{-1}}{\sqrt{n}}\right)\beta + \ln\left(\frac{\beta}{\sinh\beta}\right)\right]. \tag{3.14}$$

Next we generalize this free energy expression for a single polymer chain to a network of chains in an elastomeric gel. Assuming inextensible, strong, covalent crosslinking bonds between the chains, straightforward considerations give the following modification of (3.11):

$$\begin{aligned}\psi_{\text{R}} = \mu_{\text{R}}^0 c_{\text{R}} + \frac{R\vartheta}{\Omega}\left[\frac{\phi_0}{\phi}\Big((1-\phi)\ln(1-\phi) + \chi\phi(1-\phi)\Big)\right] \\ + (Nk_B\vartheta)\, n\left[\left(\frac{\bar{\lambda}\lambda_b^{-1}}{\sqrt{n}}\right)\beta + \ln\left(\frac{\beta}{\sinh\beta}\right)\right] - (Nk_B\vartheta)\left(\frac{\sqrt{n}}{3\lambda_b}\beta_0\right)\ln J + \Big(Nn\hat{\varepsilon}_b(\lambda_b) + \hat{\varepsilon}_{\text{Rvol}}(J^e)\Big),\end{aligned} \tag{3.15}$$

with

$$\beta \overset{\text{def}}{=} \mathcal{L}^{-1}\left(\frac{\bar{\lambda}\lambda_b^{-1}}{\sqrt{n}}\right), \qquad \text{and} \qquad \beta_0 \overset{\text{def}}{=} \mathcal{L}^{-1}\left(\frac{\lambda_b^{-1}}{\sqrt{n}}\right). \tag{3.16}$$

Note that in (3.15) and (3.16) it is the modified stretch-measure ($\bar{\lambda}\lambda_b^{-1}$) which gives rise to changes in the entropy of the network.

Let

$$\varepsilon_{\mathrm{R}} = Nn\hat{\varepsilon}_b(\lambda_b) \tag{3.17}$$

denote the internal energy density of an elastomeric network due to bond stretching. Further, let λ_b^f denote a critical value of bond stretch when a Kuhn segment fails, and denote the corresponding value of the dissociation energy for a single Kuhn segment by

$$\varepsilon_b^f \stackrel{\text{def}}{=} \hat{\varepsilon}_b(\lambda_b^f). \tag{3.18}$$

Then, as a simple criterion for failure of a "material point" of an elastomeric network due to chain-scission, Mao et al. (2017b) proposed that failure occurs when $\varepsilon_{\mathrm{R}} = \varepsilon_{\mathrm{R}}^f$, where

$$\varepsilon_{\mathrm{R}}^f \stackrel{\text{def}}{=} Nn\varepsilon_b^f \tag{3.19}$$

represents the energy of per unit volume when all Kuhn segments in a network at a "material point" are broken.

Remark. This failure criterion of Mao et al. (2017b) essentially assumes that all Kuhn segments are uniformly stretched and that they all fail simultaneously. This is a significant assumption, because at the microscopic level the chains are subject to thermal fluctuations and one expects that such fluctuations will lead to failure of a single bond rather than all the bonds simultaneously. However, to construct a simple and tractable model of failure at the macroscopic level, we neglect such complications arising from thermal fluctuations, and adopt the failure criterion of Mao et al. (2017b); we argue for its plausibility on the grounds that the binding energy of backbone units of typical polymers is large in comparison to the average thermal energy at room temperature.

3.1.3. Specialized form for the free energy accounting for bond stretch and damage

We account for damage by using the field $d \in [0, 1]$ and modify the free-energy function (3.15) to read as,

$$\begin{aligned}\psi_{\mathrm{R}} = {} & \mu_{\mathrm{R}}^0 c_{\mathrm{R}} + \frac{R\vartheta}{\Omega}\left[\frac{\phi_0}{\phi}\Big((1-\phi)\ln(1-\phi) + \chi\phi(1-\phi)\Big)\right] \\ & + (Nk_B\vartheta)\, n\left[\left(\frac{\bar{\lambda}\lambda_b^{-1}}{\sqrt{n}}\right)\beta + \ln\left(\frac{\beta}{\sinh\beta}\right)\right] - (Nk_B\vartheta)\left(\frac{\sqrt{n}}{3\lambda_b}\beta_0\right)\ln J \\ & + g(d)\underbrace{\Big(Nn\hat{\varepsilon}_b(\lambda_b) + \hat{\varepsilon}_{\mathrm{Rvol}}(J^e)\Big)}_{\equiv\hat{\varepsilon}_{\mathrm{R}}^0(\lambda_b, J^e)} + \hat{\varepsilon}_{\mathrm{R,nonloc}}(\nabla d).\end{aligned} \tag{3.20}$$

As particular forms for the functions $\hat{\varepsilon}_b(\lambda_b)$ and $\hat{\varepsilon}_{\mathrm{Rvol}}(J^e)$ we choose the simple energies,

$$\hat{\varepsilon}_b(\lambda_b) = \frac{1}{2}E_b(\lambda_b - 1)^2, \qquad \hat{\varepsilon}_{\mathrm{Rvol}}(J^e) = \frac{K}{8}(J^e - J^{e-1})^2, \tag{3.21}$$

where $E_b > 0$ denote the stiffness of a Kuhn segment, $K > 0$ a bulk modulus for intermolecular interactions.

Remark. In our finite element simulations we encountered some convergence difficulties with the simple quadratic form,

$$\hat{\varepsilon}_{\mathrm{Rvol}}(J^e) = \frac{1}{2}K(J^e - 1)^2,$$

of the volumetric internal energy at late stages of the damage. Accordingly, in our computations we have used the alternate form $(3.21)_2$ which reduces to a simple quadratic energy as $J^e \to 1$,

$$\hat{\varepsilon}_{\mathrm{Rvol}}(J^e) = \frac{K}{8}(J^e - J^{e-1})^2 = \frac{K}{8}(J^e - 1)^2\left(1 + \frac{1}{J^e}\right)^2 \approx \frac{1}{2}K(J^e - 1)^2. \tag{3.22}$$

If for some numerical reason J^e becomes large during the iteration process, then the particular form $(3.21)_2$ leads to a softer response (see Schröder and Neff, 2003). The particular form of the volumetric internal energy is not crucial for elastomeric gels in which the volume changes due to elastic deformation are typically quite small relative to distortional deformations.

Thus, denoting the undamaged part of the internal energy in (3.20) by $\hat{\varepsilon}_{\mathrm{R}}^0(\lambda_b, J^e)$, we have

$$\hat{\varepsilon}_{\mathrm{R}}^0(\lambda_b, J^e) = \frac{1}{2}\bar{E}_b(\lambda_b - 1)^2 + \frac{K}{8}(J^e - J^{e-1})^2, \tag{3.23}$$

where we have introduced the notation,

$$\bar{E}_b \stackrel{\text{def}}{=} NnE_b, \tag{3.24}$$

for a macroscopic measure of bond-stiffness.

The function $g(d)$ describes the degradation of the internal energy storage capacity of the material, with the properties

$$g(0) = 1, \quad g(1) = 0, \quad \text{and} \quad g'(1) = 0. \tag{3.25}$$

A widely-used degradation function is

$$g(d) = (1-d)^2; \tag{3.26}$$

we adopt it here.

The term $\hat{\varepsilon}_{\mathrm{R,nonloc}}(\nabla d)$ in the internal energy density is the nonlocal contribution

$$\hat{\varepsilon}_{\mathrm{R,nonloc}}(\nabla d) = \frac{1}{2}\,\varepsilon_{\mathrm{R}}^{f}\,\ell^2\,|\nabla d|^2, \tag{3.27}$$

with $\varepsilon_{\mathrm{R}}^{f}$ the macroscopic bond failure energy defined in (3.19). Also the parameter ℓ represents an intrinsic material length scale in our gradient damage theory for elastomeric gels.

With these specializations, and writing

$$G_0 \stackrel{\text{def}}{=} N k_B \vartheta, \tag{3.28}$$

for a ground-state shear modulus, the expression for the free energy may be written as

$$\begin{aligned}\psi_{\mathrm{R}} &= \mu_{\mathrm{R}}^{0} c_{\mathrm{R}} + \frac{R\vartheta}{\Omega}\left[\frac{\phi_0}{\phi}\Big((1-\phi)\ln(1-\phi) + \chi\phi(1-\phi)\Big)\right] \\ &\quad + G_0\, n\left[\left(\frac{\bar{\lambda}\lambda_b^{-1}}{\sqrt{n}}\right)\beta + \ln\left(\frac{\beta}{\sinh\beta}\right) - \left(\frac{1}{3\lambda_b\sqrt{n}}\beta_0\right)\ln J\right] \\ &\quad + (1-d)^2 \underbrace{\left(\tfrac{1}{2}\bar{E}_b(\lambda_b-1)^2 + \tfrac{K}{8}(J^e - J^{e-1})^2\right)}_{\equiv \hat{\varepsilon}_{\mathrm{R}}^{0}(\lambda_b, J^e)} + \frac{1}{2}\,\varepsilon_{\mathrm{R}}^{f}\,\ell^2\,|\nabla d|^2,\end{aligned} \tag{3.29}$$

with

$$\beta \stackrel{\text{def}}{=} \mathcal{L}^{-1}\left(\frac{\bar{\lambda}\lambda_b^{-1}}{\sqrt{n}}\right), \qquad \text{and} \qquad \beta_0 \stackrel{\text{def}}{=} \mathcal{L}^{-1}\left(\frac{\lambda_b^{-1}}{\sqrt{n}}\right). \tag{3.30}$$

Remark. An important physical consideration in our specialization above is that the degradation function $g(d) = (1-d)^2$ only degrades the internal energy $\hat{\varepsilon}_{\mathrm{R}}^{0}(\lambda_b, J^e)$ of the gel and not the entropic contributions. Thus, as $d \to 1$, the internal energy part $(1-d)^2\hat{\varepsilon}_{\mathrm{R}}^{0}(\lambda_b, J^e)$ will become zero. Even though we do not directly degrade the entropic part of the free energy, as $d \to 1$, the entropic part also goes to zero since $\lambda_b \to \infty$.

3.2. Specialized form for the Ginzburg–Landau evolution equation for the effective bond stretch λ_b

Recall (2.66), viz.

$$\hat{\kappa}_b(\mathbf{\Lambda})\,\dot{\lambda}_b = -\frac{\partial\,\hat{\psi}_{\mathrm{R}}(\mathbf{\Lambda})}{\partial\lambda_b}, \tag{3.31}$$

with $\kappa_b = \hat{\kappa}_b(\mathbf{\Lambda}) > 0$ a kinetic modulus.

As the damage variable $d \to 1$, the bond stretch λ_b also changes dramatically and eventually $\lambda_b \to \infty$. We use a specialized form of $\hat{\kappa}_b(\mathbf{\Lambda})$ to limit any dynamic effects of the breaking of bonds of the polymer chains. Since $\lambda_b \in [1, \infty)$, λ_b is not a suitable order parameter to characterize the phase transition associated with the bond-scission process. The simplest choice of an order parameter to describe this transition is the inverse of λ_b which lies in the bounded range $\lambda_b^{-1} \in [0, 1]$. A simple Ginzburg–Landau equation for the order parameter λ_b^{-1} is

$$\xi_b\,\dot{\overline{\lambda_b^{-1}}} = -\frac{\partial\,\hat{\psi}_{\mathrm{R}}(\mathbf{\Lambda})}{\partial\lambda_b^{-1}}, \tag{3.32}$$

with $\xi_b > 0$ a positive-valued kinetic modulus. Since $\dot{\overline{\lambda_b^{-1}}} = \lambda_b^{-2}\dot{\lambda}_b$ and $d\lambda_b^{-1} = \lambda_b^{-2}d\lambda_b$, (3.32) may be written as

$$\left(\xi_b\lambda_b^{-4}\right)\dot{\lambda}_b = -\frac{\partial\,\hat{\psi}_{\mathrm{R}}(\mathbf{\Lambda})}{\partial\lambda_b}, \tag{3.33}$$

which is of the general form (3.31), with

$$\kappa_b = \xi_b\lambda_b^{-4}. \tag{3.34}$$

3.3. Specialized form for ϖ_{diss}

Next we specialize the expression for the dissipative microforce $\varpi_{\rm diss}$ that expends power through $\dot{d}$.[5] The dissipative microforce is partitioned into a rate-independent part and a rate-dependent part through

$$\varpi_{\rm diss} = \underbrace{\hat{\alpha}(\mathbf{\Lambda})}_{\text{rate-independent}} + \underbrace{\hat{\zeta}(\mathbf{\Lambda})\dot{d}}_{\text{rate-dependent}} . \tag{3.35}$$

Based on physical model of Mao et al. (2017b), the rate-independent part of the dissipative microforce α is the sum of the contributions from each chain given by (3.19), and is given by

$$\alpha = \varepsilon_{\rm R}^f. \tag{3.36}$$

The rate-dependent contribution to the dissipative microforce is here taken to be simply described by a constant kinetic modulus $\zeta > 0$, with the rate-independent limit given by $\zeta \to 0$.

3.4. Specialized form for the evolution equation for d

Using the specialized free energy (3.29) and the specialization for $\varpi_{\rm diss}$ above, Eq. (2.68), which gives the evolution of d, becomes

$$\zeta \dot{d} = 2(1-d)\hat{\varepsilon}_{\rm R}^0(\lambda_b, J^e) + \varepsilon_{\rm R}^f \ell^2 \Delta d - \varepsilon_{\rm R}^f. \tag{3.37}$$

Remark. Consider the rate-independent limit ($\zeta = 0$) in the absence of any gradient in the damage field d. Then (3.37) reduces to

$$0 = 2(1-d)\hat{\varepsilon}_{\rm R}^0(\lambda_b, J^e) - \varepsilon_{\rm R}^f. \tag{3.38}$$

Using the fact that d lies in the range $d \in [0, 1]$, (3.38) gives that

$$d = \begin{cases} 0, & \text{if } \hat{\varepsilon}_{\rm R}^0(\lambda_b, J^e) \le \varepsilon_{\rm R}^f/2, \\ 1 - \dfrac{\varepsilon_{\rm R}^f/2}{\hat{\varepsilon}^0(\lambda_b, J^e)} & \text{if } \hat{\varepsilon}^0(\lambda_b, J^e) > \varepsilon_{\rm R}^f/2. \end{cases} \tag{3.39}$$

The evolution equation (3.37) can be rewritten to enforce the constraint $d \in [0, 1]$ in a simple way. Add and subtract the term $\varepsilon_{\rm R}^f d$ to (3.37) to get,

$$\zeta \dot{d} = 2(1-d)\big(\hat{\varepsilon}^0(\lambda_b, J^e) - \varepsilon_{\rm R}^f/2\big) - \varepsilon_{\rm R}^f\big[d - \ell^2 \Delta d\big].$$

Since $\hat{\varepsilon}_{\rm R}^0(\lambda_b, J^e)$ is the major driving energy for the evolution of d, the constraint $d \in [0, 1]$ is satisfied if the equation above is modified to read as,

$$\zeta \dot{d} = 2(1-d)\big\langle\hat{\varepsilon}_{\rm R}^0(\lambda_b, J^e) - \varepsilon_{\rm R}^f/2\big\rangle - \varepsilon_{\rm R}^f\big[d - \ell^2 \Delta d\big], \tag{3.40}$$

where $\langle\bullet\rangle$ are Macauley brackets, i.e.,

$$\langle x\rangle = \begin{cases} 0, & x < 0, \\ x, & x \ge 0. \end{cases}$$

In this form, a threshold for the driving energy for damage is made explicit.

At this stage in the development of the model for the evolution of d, the irreversible nature of scission is not yet reflected in the model. To this end, we replace the term $\langle\hat{\varepsilon}_{\rm R}^0(\lambda_b, J^e) - \varepsilon_{\rm R}^f/2\rangle$ in (3.40) with the monotonically increasing history function (cf., Miehe et al., 2010),

$$\mathcal{H}(t) \stackrel{\rm def}{=} \max_{s\in[0,t]} \big\langle\hat{\varepsilon}_{\rm R}^0(\lambda_b(s), J^e(s)) - \varepsilon_{\rm R}^f/2\big\rangle. \tag{3.41}$$

The Ginzburg–Landau evolution equation for d (2.68) may then be written in a form similar to that found in the numerous papers by Miehe and co-workers on phase-field fracture (cf., e.g., Miehe and Schänzel, 2014; Miehe et al., 2010; Raina and Miehe, 2016),[6]

$$\zeta \dot{d} = 2(1-d)\mathcal{H} - \varepsilon_{\rm R}^f\big[d - \ell^2 \Delta d\big]. \tag{3.42}$$

The free energy (3.29) gives the vector microstress as $\boldsymbol{\xi} = \varepsilon_{\rm R}^f \ell^2 \nabla d$, so that the boundary conditions conditions (2.71) for the partial differential equation (3.42) may be written as,

$$\dot{d} = 0 \quad \text{on } \mathcal{S}_d \times [0, T], \qquad \text{and} \qquad (\nabla d)\cdot \mathbf{n}_{\rm R} = 0 \quad \text{on } \partial\, \mathrm{B} \setminus \mathcal{S}_d \times [0, T]. \tag{3.43}$$

[5] Cf. Eqs. (2.57) and $(2.58)_1$.

[6] However, our derivation of (3.42) differs in substantial detail from that in the papers by Miehe et al.

The latter boundary condition thus means that the gradient of phase field ∇d is taken to be perpendicular to the normal $\mathbf{n}_{\mathrm{R}}$ to the surface $\partial \mathrm{B} \setminus \mathcal{S}_d$, so that any "diffuse crack" intersects the boundary in a perpendicular fashion. Such a boundary condition is widely used in gradient damage theories in the literature (cf., e.g., Miehe et al., 2010).

3.5. Specialization of the referential fluid mobility tensor M

We note that with

$$c \overset{\text{def}}{=} J^{-1} c_{\mathrm{R}} \qquad \text{and} \qquad \mathbf{j} \overset{\text{def}}{=} J^{-1} \mathbf{F} \mathbf{j}_{\mathrm{R}}, \tag{3.44}$$

respectively, denoting the fluid content measured per unit volume of the deformed body, and the fluid flux measured per unit area of the deformed body per unit time, the referential balance law (2.15) may be expressed spatially as,

$$\dot{c} = -\mathrm{div}\mathbf{j}. \tag{3.45}$$

At present not much is known experimentally about the precise constitutive equation for the flux $\mathbf{j}$. Here we use a simple form to capture the essence of the diffusion of the fluid in the gel. Specifically, we assume that the spatial flux depends linearly on the spatial gradient of the chemical potential, with the mobility tensor spherical, so that

$$\mathbf{j} = -m \,\mathrm{grad}\, \mu, \tag{3.46}$$

with

$$m = \hat{m}(c, d, \vartheta) > 0 \tag{3.47}$$

a positive-valued mobility coefficient. The assumption that the spatial mobility tensor is spherical, $m\mathbf{1}$, implies that the fluid diffusion always remains isotropic and is not influenced by deformation or damage of the gel. We assume further that the spatial scalar mobility m at a given temperature ϑ is given by,

$$m = \frac{Dc}{R\vartheta} \qquad \text{with} \qquad D = \hat{D}(d) > 0, \tag{3.48}$$

where D represents a diffusion coefficient with units of m^2/s. Finally, using the transformations $(3.44)_2$ and $\mathrm{grad}\,\mu = \mathbf{F}^{-\top}\nabla\mu_{\mathrm{R}}$, the spatial relation (3.46) may be converted to its referential counterpart,

$$\mathbf{j}_{\mathrm{R}} = -\mathbf{M}\nabla\mu_{\mathrm{R}}, \tag{3.49}$$

with

$$\mathbf{M} = J\left(\frac{Dc}{R\vartheta}\right)\mathbf{C}^{-1} \qquad \text{with} \qquad D = \hat{D}(d) > 0, \tag{3.50}$$

a positive-semidefinite referential mobility tensor. The precise dependence of the damage on the diffusion coefficient is not known; we expect that as the damage d increases then so also does the diffusion coefficient D, but in our numerical calculations — for simplicity — we take D to be a constant.[7]

4. Summary of the governing equations for the specialized theory

1. **Balance of forces**: Neglecting body forces, balance of forces requires

$$\mathrm{Div}\mathbf{T}_{\mathrm{R}} = \mathbf{0}, \tag{4.1}$$

with $\mathbf{T}_{\mathrm{R}}$ given by

$$\mathbf{T}_{\mathrm{R}} = \bar{G}\mathbf{F} - \bar{G}_0\mathbf{F}^{-\top} + (1-d)^2\frac{1}{4}K(J^{e2} - J^{e-2})\mathbf{F}^{-\top}, \tag{4.2}$$

where

$$\begin{aligned} &\bar{G} \overset{\text{def}}{=} G_0\left(\frac{\sqrt{n}}{3\bar{\lambda}\lambda_b}\right)\beta, \qquad G_0 = Nk_{\mathrm{B}}\vartheta, \qquad \beta = \mathcal{L}^{-1}\left(\frac{\bar{\lambda}\lambda_b^{-1}}{\sqrt{n}}\right), \\ &\bar{G}_0 \overset{\text{def}}{=} G_0\left(\frac{\sqrt{n}}{3\lambda_b}\right)\beta_0, \qquad \beta_0 \overset{\text{def}}{=} \mathcal{L}^{-1}\left(\frac{\lambda_b^{-1}}{\sqrt{n}}\right), \end{aligned} \tag{4.3}$$

and $\mathcal{L}^{-1}(\cdot)$ is the inverse of the Langevin function $\mathcal{L}(x) = \coth x - x^{-1}$.

[7] This assumption is approximately valid in the numerical simulations that we report in Section 5, since in these simulations the rupture happens very quickly, and any dependency of the mobility on damage may be neglected.

The bond-stretch λ_b is solved by integrating the evolution equation

$$\left(\frac{\xi_b}{G_0 n}\lambda_b^{-3}\right)\dot{\lambda}_b = -\left[(1-d)^2\frac{\bar{E}_b}{G_0 n}(\lambda_b - 1)\lambda_b - \frac{\bar{\lambda}\lambda_b^{-1}}{\sqrt{n}}\beta + \frac{\lambda_b^{-1}}{3\sqrt{n}}\left(\beta_0 + \frac{\partial \beta_0}{\partial r_0}r_0\right)\ln J\right], \tag{4.4}$$

in which

$$\bar{E}_b = N\,n\,E_b, \qquad \text{and} \qquad r_0 \stackrel{\text{def}}{=} \frac{1}{\sqrt{n}\,\lambda_b}.$$

2. **Balance of fluid concentration**:

$$\dot{c}_{\mathrm{R}} = -\mathrm{Div}\,\mathbf{j}_{\mathrm{R}}, \tag{4.5}$$

with $\mathbf{j}_{\mathrm{R}} = -\mathbf{M}\nabla\mu_{\mathrm{R}}$, with the mobility given by (3.50) and the chemical potential by

$$\mu_{\mathrm{R}} = \mu_{\mathrm{R}}^0 + R\vartheta[\ln(1-\phi) + \phi + \chi\phi^2] - (1-d)^2 J^{s-1}\frac{1}{4}K(J^{e2} - J^{e-2})\Omega. \tag{4.6}$$

3. **Evolution equation for the damage variable** d:

$$\zeta\dot{d} = 2(1-d)\mathcal{H} - \varepsilon_{\mathrm{R}}^f\left[d - \ell^2\Delta d\right], \tag{4.7}$$

in which

$$\varepsilon_{\mathrm{R}}^f = N\,n\,\varepsilon_b^f, \tag{4.8}$$

is energy required to fail the Kuhn segments, ℓ is a material length scale, and $\mathcal{H}$ is a history functional defined by

$$\mathcal{H}(t) \stackrel{\text{def}}{=} \max_{s\in[0,t]}\left\langle \hat{\varepsilon}_{\mathrm{R}}^0(\lambda_b(s), J^e(s)) - \varepsilon_{\mathrm{R}}^f/2\right\rangle, \tag{4.9}$$

where at each $s \in [0, t]$,

$$\hat{\varepsilon}_{\mathrm{R}}^0(\lambda_b(s), J^e(s)) = \frac{1}{2}N\,n\,E_b(\lambda_b(s) - 1)^2 + \frac{1}{8}K(J^e(s) - J^{e-1}(s))^2. \tag{4.10}$$

The theory involves the following material parameters:

$$N, \quad n, \quad E_b, \quad K, \quad \xi_b, \qquad \mu_{\mathrm{R}}^0, \quad \Omega, \quad \chi, \quad D, \qquad \varepsilon_b^f, \quad \ell, \quad \text{and} \quad \zeta. \tag{4.11}$$

Here, N is the number of chains per unit volume; n represents number of links in a chain; E_b represents a modulus related to stretching of the bonds (Kuhn segments) of the polymer molecules; K, represents the bulk modulus of the material; ξ_b is a kinetic modulus for the evolution of the bond stretch; μ_{R}^0 is the reference chemical potential of the solvent; Ω is the molar volume of the diffusing fluid; χ is the Flory–Huggins interaction parameter between the polymer and solvent; D is the diffusivity of the fluid molecules; ε_b^f, a bond dissociation energy per unit volume; ℓ is a characteristic length scale of the gradient damage theory under consideration; and ζ is a kinetic modulus for the evolution of the damage.

In the numerical simulations to described in Section 5, instead of the parameter list (4.11), we use the parameter list,

$$\begin{aligned} &\text{Network parameters}: \quad G_0 = Nk_B\vartheta, \quad n, \quad \bar{E}_b = NnE_b, \quad K, \quad \xi_b, \quad \varepsilon_{\mathrm{R}}^f = Nn\varepsilon_b^f, \quad \ell, \quad \text{and} \quad \zeta, \\ &\text{Fluid diffusion parameters}: \quad \mu_{\mathrm{R}}^0, \quad \Omega, \quad \chi, \quad \text{and} \quad D, \end{aligned} \tag{4.12}$$

where G_0 is the ground-state shear modulus for the polymer network, $\bar{E}_b$ is a bond-stiffness parameter for the network, and $\varepsilon_{\mathrm{R}}^f$ represents the energy per unit volume for the dissociation of all the Kuhn segments in a network.

The boundary conditions for these partial differential equations have been discussed previously in Section 2.12.

5. Numerical implementation. Representative simulations

We have numerically implemented our theory in the open-source finite element code MOOSE (Gaston et al., 2009) by writing our own application to solve 3D, plane-strain, plane-stress, axisymmetric problems. MOOSE uses a sophisticated nonlinear solver technology, and it may be massively parallelized. Using this new numerical capability, in this section we report on some representative simulations of coupled diffusion-deformation-fracture of a polymeric gel. All simulations were performed on a parallelized linux cluster with $\sim$100 cores. The simulations presented below took $\sim$ 6 hours to complete. Visualization of the results was performed by using the open-source code ParaView (Ayachit, 2015).

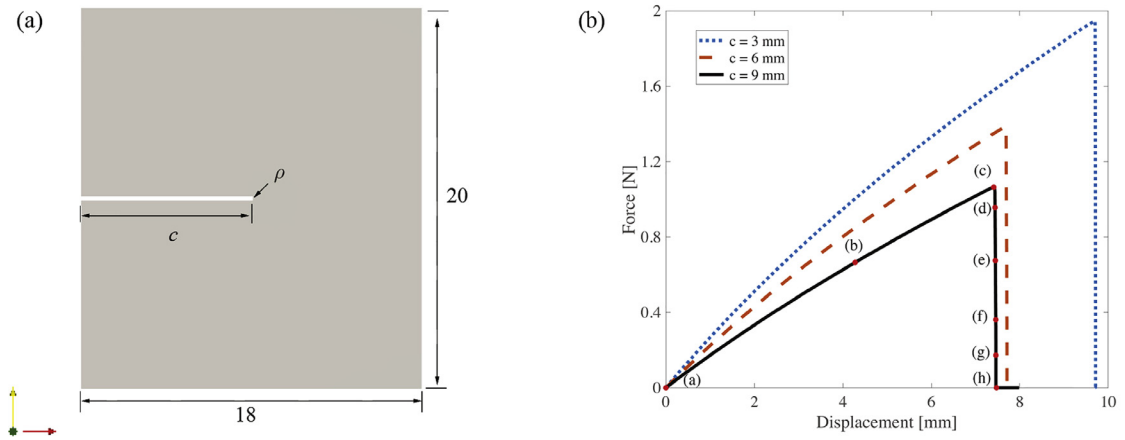

Fig. 1. (a) Schematic of the single-edge-notch specimen geometry; all dimensions are in mm. The thickness of the sample is 1 mm; the notch length is denoted by c; and $\rho = 0.1$ mm is the notch-root radius. (b) Calculated force-displacement curves for $c = 3, 6, 9$ mm. Contour plots for the damage variable d and the polymer volume fraction ϕ at points (a) through (h) on the load displacement curve for a specimen with $c = 9$ mm are shown in Fig. 2 and Fig. 3.

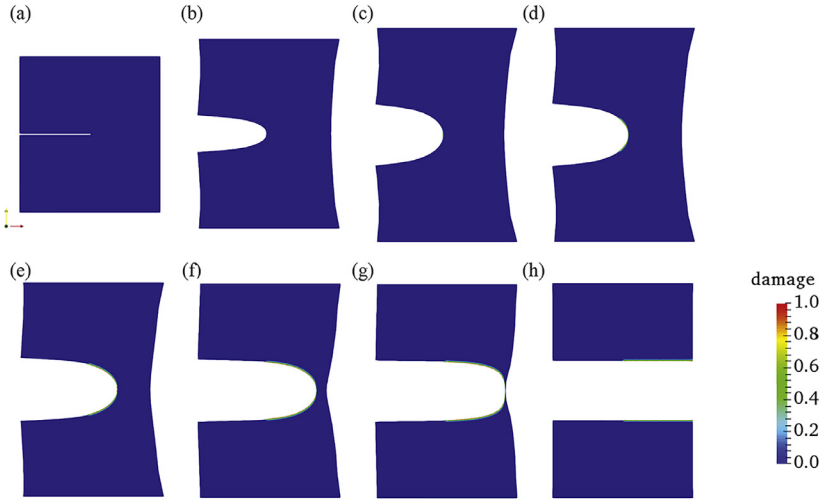

Fig. 2. Images of the deformed geometry with contour plots of the damage variable d. To aid visualization of the damage, elements with an average value of $d > 0.99$ are removed from the plots. Since the length scale $\ell = 100\,\mu$m is very small when compared with the overall dimension of the specimen (~ 20 mm), the damage zone is barely visibly in this this sequence of contour plots for d.

5.1. Single-edge-notch Mode-I loading under plane-stress conditions with different notch lengths

We begin with a study of fracture in single-edge-notch specimens with different notch lengths, under plane-stress Mode-I loading conditions. Fig. 1(a) shows a schematic of the specimen geometry. The overall size of the notched sheet sample is 20 mm × 18 mm in the plane, and the sheet is 1 mm thick. We consider specimens with notch lengths $c = 3$, 6, and 9 mm; the initial root-radius of the notch is fixed at 0.1 mm. The temperature is kept constant at $\vartheta = 300$K, and the initial volume fraction of polymer is set at $\phi_0 = 0.5$. The displacement of the bottom edge of the specimen is fixed, while the top-edge is prescribed a displacement at a nominal stretch rate of 1×10^{-3}/s. We use a zero-fluid-flux boundary condition on all the boundaries of the specimen, so that no fluid goes into or out of the specimen — but the fluid is allowed to diffuse within the specimen.[8]

The material parameters used in our simulations are shown in Table 1. For simplicity, the reference chemical potential is set to $\mu_R^0 = 0$. In order to study the effects of diffusion on deformation and fracture,

- we have purposely chosen a rather high value of the diffusivity D,

[8] Our theory and numerical procedures allow for boundary conditions that allow for fluid influx or efflux on the boundary, but in this initial study we do not consider such boundary conditions as they complicate the situation by introducing another time-scale in the problem. We leave a study of injection and evaporation of fluid from the surface of the body on gel-fracture to a later publication.

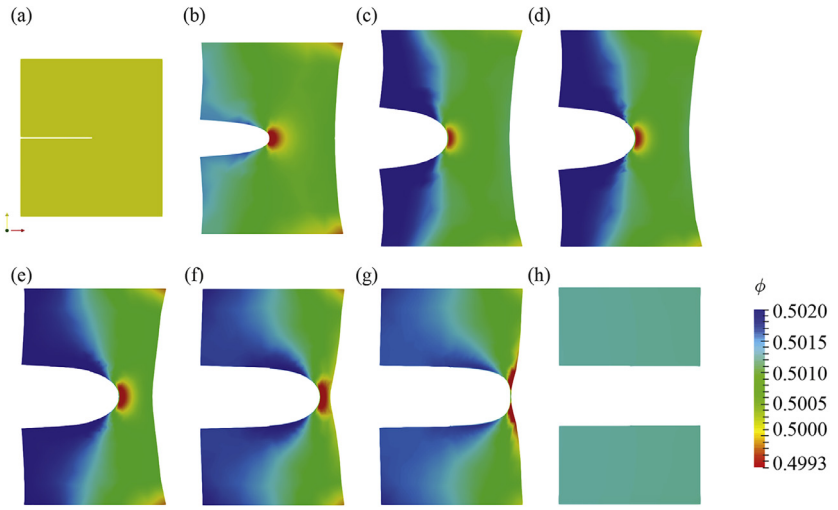

Fig. 3. Images of the deformed geometry with contour plots of the volume fraction of polymer ϕ. To aid visualization of the damage, elements with an average value of $d > 0.99$ are removed from the plots.

Table 1
Representative values of the material parameters used in the simulations.

$G_0 = Nk_B\vartheta$	n	$\bar{E}_b = NnE_b$	K	$\varepsilon_R^f = Nn\varepsilon_b^f$	ℓ	ξ_b and ζ
0.1 MPa	4	5 MPa	10 MPa	1 MPa	100 μm	1 kPa · s
μ_R^0	Ω	χ	D			
0	1×10^{-4} m^3/mol	0.1	1×10^{-3}m^2/s			

in order to represent fast diffusion within the notched-specimen, relative to the time-scale at which it is being extended (a nominal stretch rate of 1×10^{-3}/s). For a systematic study of the effect of the fluid diffusivity on fracture, see the next Section 5.2.[9]

Fig. 1(b) shows the calculated force-displacement curves for notches with initial lengths of $c = 3, 6, 9$ mm. As expected, as the initial length of the notch increases the overall force level becomes lower, and the stretch at which final fracture occurs becomes smaller. Contour plots for the damage variable d and the polymer volume fraction ϕ at points (a) through (h) on the load displacement curve for a specimen with $c = 9$ mm are shown in Figs. 2 and 3, respectively.

Fig. 2 shows the deformed geometry at points (a) through (h) on the force-displacement curve in Fig. 1(b), together with contours of the damage variable d. To aid visualization of the damage, elements with an average value of $d > 0.99$ are not plotted. Since the length scale $\ell = 100\,\mu$m is very small when compared with the overall dimension of the specimen ($\sim$20 mm), the damage zone is barely visibly in this this sequence of plots. Fig. 2(a) is the initial configuration. As the sample is stretched to (b) the notch is blunted, but no damage has initiated. Damage initiates when the sample is stretched further to a displacement level of $\sim$7 mm (a point just before (c)), but the force is still increasing, and it is after another $\sim$0.5 mm of extension that the force reaches a peak at point (c) in the force-displacement curve, and from the contour of damage shown in Fig. 2(c), a small damage zone ahead of the notch becomes observable. Further stretching begins the rupture process, and Fig. 2(d) through (h) show this progressive rupturing, with (h) showing the final failed configuration. Note from Fig. 1(b) that the force at stage (h) stage is essentially zero.

Fig. 3 shows the deformed geometry with contour plots of the volume fraction of polymer ϕ corresponding to the points (a) through (h) in Fig. 1(b). Again, to aid visualization of the damage, elements with an average value of $d > 0.99$ are removed from the plots. At the initial stage (a) the volume fraction of polymer ϕ has a constant value $\phi_0 = 0.5$. Fig. 3 shows that as the sample is stretched the volume fraction of polymer ahead of the notch-tip decreases, with a zone of low volume fraction of polymer moving with notch-tip. The region of lower polymer volume fraction — and therefore higher fluid concentration — increases the propensity to damage and failure because of the lower number of polymer chains in such regions which are also more highly stretched. After full rupture, the polymer concentration in the two halves of the specimen once again becomes almost uniform (except in the fully-damaged and deleted portion).

[9] Also, in our numerical calculations we have used a value of the bulk modulus K which is 100 times larger than the ground state shear modulus G_0; this corresponds to a ground-state Poisson's ratio of $\nu = 0.495$, which approximates an elastically incompressible material. We tried using larger values of K relative to that of G_0, but that slowed down our numerical procedures considerably. So in all the calculations reported here we have used $K/G_0 = 100$.

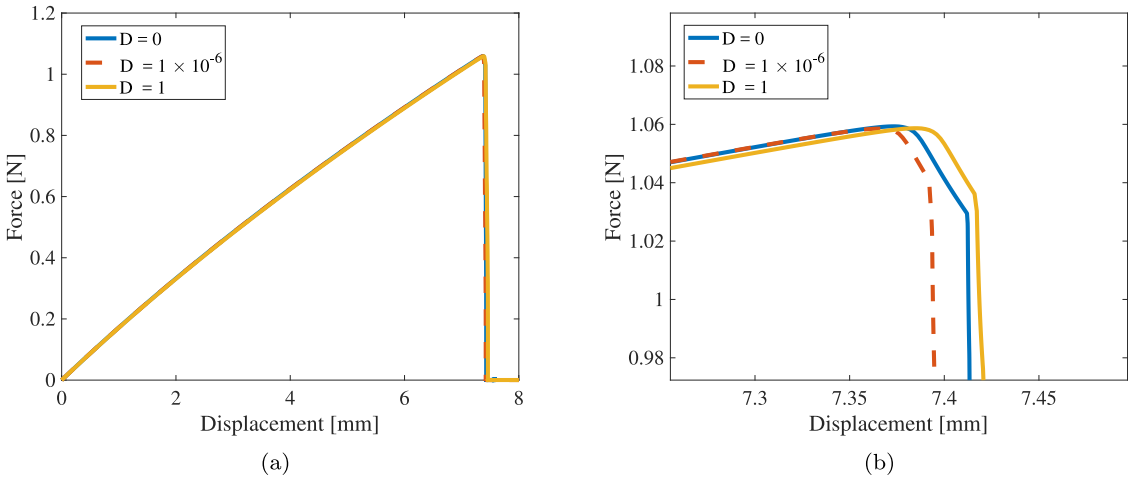

Fig. 4. (a) The effect of diffusivity D on the force-displacement curve of a single-edge-notch specimen with notch length $c = 9$ mm. The nominal stretch rate of the specimen is 1×10^{-3}/s for all cases. (b) A zoom in of the region in the vicinity of load-drop.

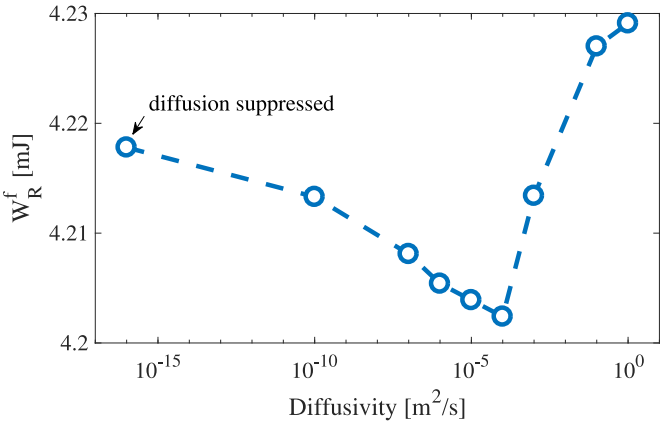

Fig. 5. The effect of diffusivity, D, on the external work needed to rupture a sample, W_{R}^f, for a specimen with notch length $c = 9$ mm. The macroscopic stretch rate is 1×10^{-3}/s for all cases.

5.2. Single-edge-notch Mode-I loading under plane-stress conditions with different diffusivities

Next, we show results from simulations for a single-edge-notch specimen with a fixed notch length of $c = 9$ mm, but with three different diffusivities,

$$D = 0, \quad 1 \times 10^{-6}, \quad \text{and} \quad 1 \quad \mathrm{m}^2/\mathrm{s}. \tag{5.1}$$

The case $D = 0$ corresponds to the fracture of a gel in which the diffusion is completely suppressed within the specimen, while $D = 1$ corresponds to very fast diffusion. As in the previous section, we prescribe no-flux boundary conditions on the boundaries of the specimen. The displacement of the bottom edge of the specimen is fixed, while the top-edge is prescribed a displacement at a nominal stretch rate of 1×10^{-3}/s.

Fig. 4(a) shows the resulting force-displacement curves for the three different diffusivities, and Fig. 4(b) shows a zoom in of the part of the force-displacement curves in the vicinity of load-drop. Fig. 4(a) shows that there are very small differences between the macroscopic load-displacement curves for the different diffusivities while the force-displacement curves are increasing, and Fig. 4(b) shows that the load-peak and its position differs for the three different diffusivities.

Let

$$W_{\mathrm{R}}^f \stackrel{\mathrm{def}}{=} \text{External work done to completely rupture the specimen.} \tag{5.2}$$

Values of W_{R}^f are calculated by integrating the area under the load-displacement curves (such as those shown in Fig. 4(a)) for the different values of the diffusivity within a wide range — $D = 0$ to $1\mathrm{m}^2/\mathrm{s}$. In Fig. 5 the value of W_{R}^f for the baseline case of $D = 10^{-16} \approx 0$ is plotted as the most left point, and the results for the other values of W_{R}^f for the different diffusivities are shown as open blue circles.

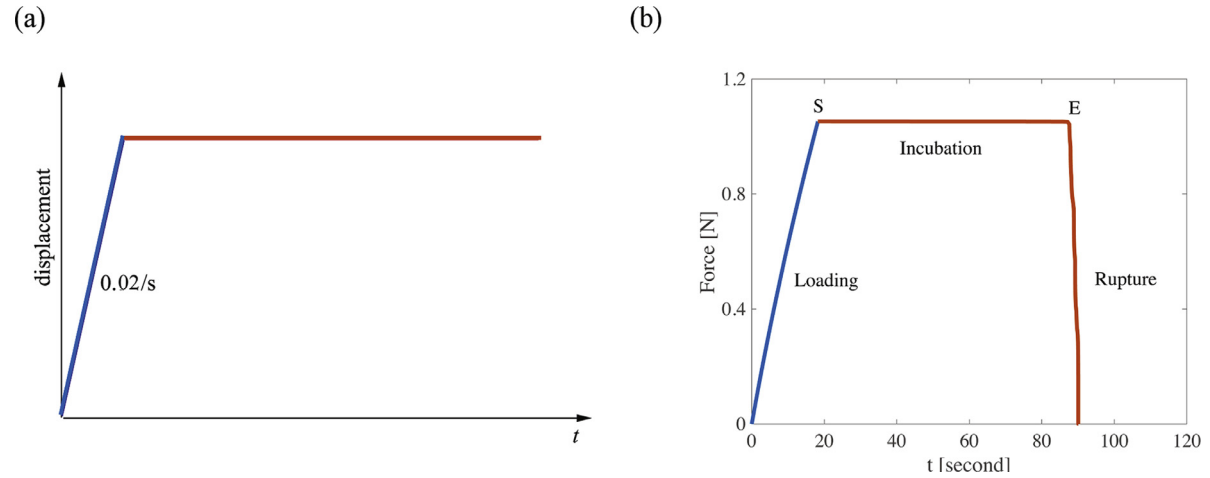

Fig. 6. Delayed-fracture in a gel due to diffusion of the fluid. (a) The macroscopic applied stretch rate is 0.02/s in the first step (blue), and 0 in the second step (red). (b). The force-time curve obtained from simulation. The incubation period is $\sim$70 seconds. (For interpretation of the references to color in this figure legend, the reader is referred to the web version of this article.)

As we have discussed earlier, diffusion of the fluid to the notch-tip region increases the propensity of the material to fracture in that region because of the smaller number of highly stretched polymer chains per unit volume, and this will cause a decrease in the value of W_{R}^{f}. However, migration of the solvent in the specimen is a dissipative process and this increases the overall energy that is dissipated in the process of rupturing of the gel, and causes an increase in W_{R}^{f}. It is these two competing mechanisms which cause the W_{R}^{f} versus D curve in Fig. 5 to first decrease and then to increase, as the diffusivity D increases.

5.3. Delayed fracture in gels. Interaction between diffusion and damage

In the previous section we have shown that by changing the diffusivity but keeping the stretch-rate constant, that our model can capture the effect of diffusion on the deformation and damage processes of gels in a single-edge-notch specimen. However, for actual gels the diffusivity cannot be substantially changed, it is always about $D \approx 1 \times 10^{-9}$ to 1×10^{-8} m^2/s; but what one can be controlled is the macroscopic stretch rate of a notched specimen. The competition between the time-scale for the stretching and the time-scale for diffusion is vividly displayed in an experiment in which a notched-sample is first rapidly stretched to a level below which damage is initiated at the notch-tip, and the macroscopic displacement is thereafter held constant. Fracture is observed to occur after a substantial period of time, as the fluid migrates in the specimen to highly-stressed region near the notch-tip. We study this interesting phenomenon of "delayed-fracture" next.

We set $D = 1 \times 10^{-8}$ m^2/s, and with all other material parameters as before, a single-edge-notch specimen with initial notch length $c = 9$ mm (cf. Fig. 1(a)) is loaded in two steps, as shown in Fig. 6(a): the applied stretch rate is 0.02/s in the first step (blue), and 0 in the second step (red). Examining Fig. 4(b) we see that the case with different diffusivity, failure starts at a displacement of $\sim$7.38 mm. Guided by these results, in our simulation we choose the total displacement imposed to sample at the end of the first step to be 7.30 mm, and thereafter hold the displacement fixed at this value. Fig. 6(b) shows the resulting force versus time curve from our simulation. Three periods are identified from this force-time curve: loading, incubation, and quick rupture. Since the initial loading rate is relatively fast, the diffusion within this loading period is limited. To understand what is happening during the incubation period, we mark the start and the end of incubation by "S" and "E" in Fig. 6(b), and compare the contours of the polymer volume fraction and damage fields for these two configurations in Fig. 7.

Fig. 7(a) and (b) shows contours of the volume fraction of polymer and damage at the start and end of the incubation time, respectively; to aid visualization, the contours of the damage and the volume fraction of polymer are displayed on the undeformed configuration. At the start of the incubation period a limited amount of damage appears at the notch-tip. While Fig. 6(b) shows the force versus time curve is essentially flat between the stages "S" and "E", Fig. 7 shows that that even though the change in the macroscopic force-time response of the sample is negligible, substantial changes in the fields ϕ and d occur during the incubation time, as the solvent diffuses to the highly-stressed notch-tip region from the rest of the specimen. As we have discussed earlier, diffusion of the fluid to the notch-tip region increases the propensity of the material to fracture in that region because of the smaller number of highly stretched polymer chains per unit volume, and this drives the damage process in the notch-tip zone. At the end of the incubation time enough damage has accumulated, and thereafter it starts to grow rapidly, the force starts to drop dramatically, and rupture occurs.

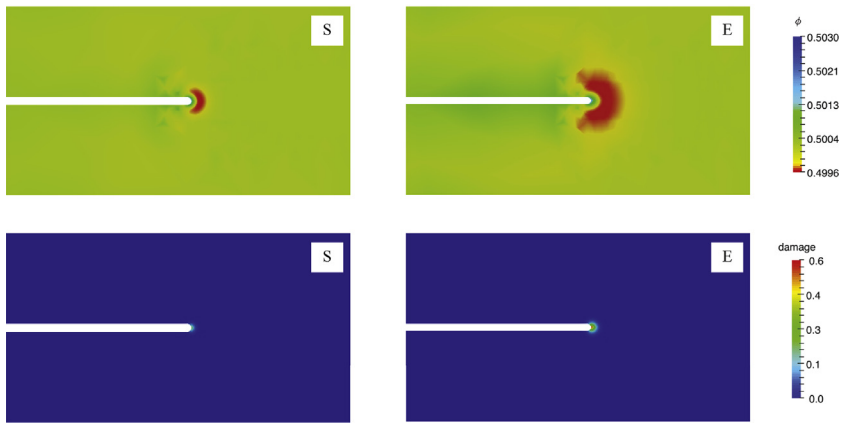

Fig. 7. (a) Contours of polymer volume fraction ϕ at the start and end of incubation time, respectively. (b) Contours of damage d at the start and end of incubation time, respectively. To aid visualization, the contours of the damage and the volume fraction of polymer are displayed on the undeformed configuration.

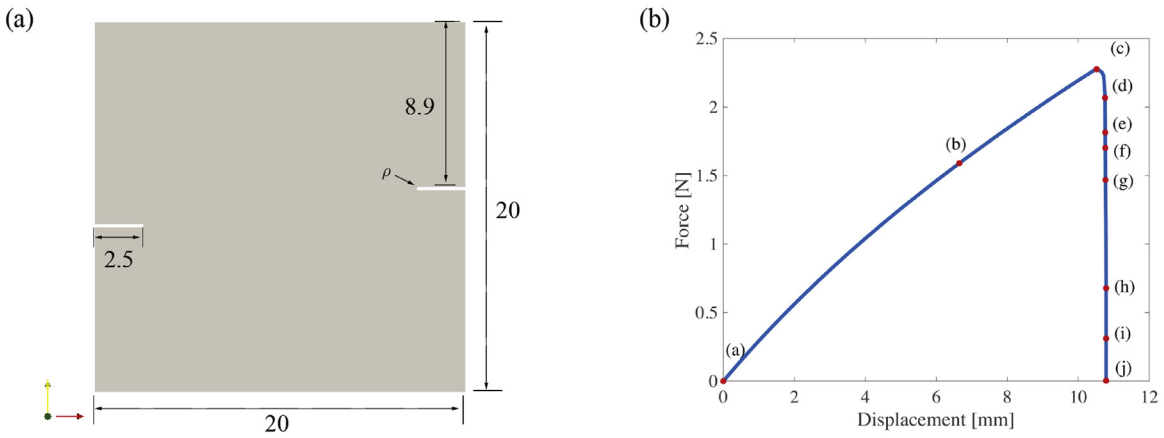

Fig. 8. (a) Schematic of the asymmetric-double-edge-notch specimen geometry; all dimensions are in mm. The thickness of the sample is 1 mm; the notches are of length $c = 2.5$ mm; and $\rho = 0.1$ mm is the notch-root radius. (b) Calculated force-displacement curve. The contour plots for the damage variable d at points (a) through (j) on the load displacement curve are shown in Fig. 9.

5.4. Fracture in an asymmetric-double-edge-notched sheet of a gel under Mode-I plane-stress loading

In this section we study fracture of an asymmetric-double-notched sheet specimen of a gel under Mode-I plane-stress loading. This example shows the powerful capability of our gradient-damage theory to model the merging of two growing notches.

Fig. 8(a) shows a schematic of the specimen geometry. The overall size of the double-edge-notched sheet sample is 20 mm × 20 mm in the plane, and the sheet is 1 mm thick. The two offset notches each have a of length $c = 2.5$ mm; the initial root-radius of the notch is 0.1 mm. As in our single-edge notch simulations in Section 5.1, the temperature is kept constant at $\vartheta = 300$K, the initial volume fraction of polymer is set to be $\phi_0 = 0.5$, and we use the same values of the material parameters as in Section 5.1. The bottom edge of the specimen is fixed, while the top-edge is prescribed a displacement at a nominal stretch rate of 1×10^{-3}/s. We use a zero-fluid-flux boundary condition on all the boundaries of the specimen, so that no fluid goes into or out of the body, but the fluid is allowed to diffuse within the specimen. Fig. 8(b) shows the calculated force-displacement curve.

The contour plots for the damage variable, d, and the polymer volume fraction ϕ at points (a) through (j) on the load displacement curve in Fig. 8(b) are shown in Fig. 9. To aid visualization of the damage, elements with an average value of $d > 0.99$ are removed from the plots. Since the length scale $\ell = 100\,\mu$m is very small compared with the overall dimension of the specimen (20 mm), the damage zone is barely visibly in this this sequence of plots. Fig. 9(a) is the initial configuration. As the sample is stretched to (b) both the notches get blunted, but no damage has initiated. Damage initiates when the sample is stretched further to a displacement of $\sim$11mm (just before state (c)), but the force is still increasing; it is only after another $\sim$1mm of extension that the force reaches a peak at point (c) in the force-displacement curve Fig. 8(b), and

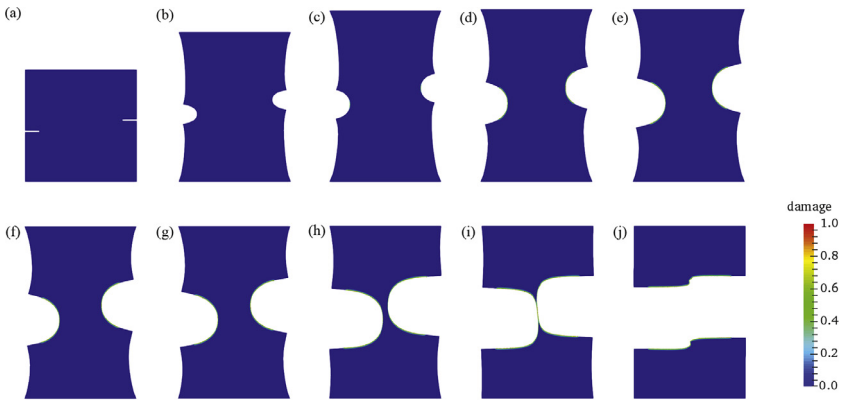

Fig. 9. The deformed geometry with contour plots of the damage variable d. To aid visualization of the damage, elements with an average value of $d > 0.99$ are removed from the plots. Since the length scale $\ell = 100\,\mu$m is very small compared with the overall dimension of the specimen (~ 20 mm), the damage zone is barely visibly in this sequence of plots.

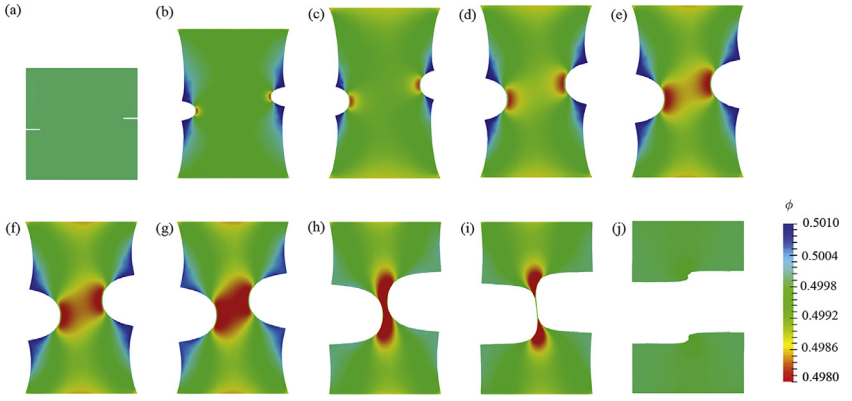

Fig. 10. The deformed geometry with contour plots of the volume fraction of polymer ϕ. To aid visualization of the damage, elements with an average value of $d > 0.99$ are removed from the plots.

from the contour of damage d shown in Fig. 9(c), a small damaged zone ahead of the notch becomes observable. Figs. 9(d) through (j) shows the subsequent rupturing process, with (j) the final failed configuration.

Fig. 10 shows contours of the volume fraction of polymer, ϕ, corresponding to the points (a) through (j) in Fig. 8(b). Again, to aid visualization of the damage, elements with an average value of $d > 0.99$ are removed from the plots. At the initial stage (a) the volume fraction of polymer ϕ has a constant value $\phi_0 = 0.5$. As the sample is stretched, cf. (b) and (c), the volume fraction of polymer ahead of both notch-tips decreases. Upon further stretching the zones of low polymer volume fraction move with the notch-tips, and since the size of these zone grows, the distance between the two zones decreases. The two zones eventually interact and merge with each other, as shown in (e) through (h). Figure (i) shows a pinching off process, which leads to final fracture into two separate pieces, as shown in (j). After final fracture the polymer volume fraction once again becomes almost uniform in the two halves of specimen (except in the fully-damaged and deleted portion).

6. Concluding remarks

We have formulated a theory for fracture of polymeric gels — a theory which accounts for the coupled effects of fluid diffusion, large deformations, damage, and also the gradient effects of damage. The particular constitutive equations for fracture of a gel proposed in our paper contain two essential new ingredients: (i) Our constitutive equation for the change in free energy of a polymer network accounts for not only changes in the entropy, but also changes in the internal energy due the stretching of the Kuhn segments of the polymer chains in the network. (ii) The damage and failure of the polymer network is taken to occur by chain-scission, a process which is driven by the changes in the internal energy of the stretched polymer chains in the network, and not directly by changes in the configurational entropy of the polymer chains.

We have numerically implemented our theory in an open-source finite element code MOOSE (Gaston et al., 2009) by writing our own application.

Using this simulation capability we have presented results form our simulations of Mode-I fracture in single-edge-notch and asymmetric-double-edge-notch geometries under plane-stress conditions. The single-edge notch geometry was used to explore the consequences of the competition between the characteristic time-scale for deformation and the characteristic time-scale for diffusion by fixing the time scale for deformation, and varying the value of the diffusivity of the fluid. While there are many operating conditions under which the characteristic time-scale for deformation is much smaller than the time-scale for diffusion, so that the diffusion of the fluid may be neglected, there are also operating conditions under which the fluid diffusion cannot be ignored. One such set of conditions occurs when a notched-specimen is stretched to a sub-critical level and thereafter the stretch is held constant; after a sufficient incubation time damage accumulates and eventually fracture occurs — a phenomenon known as "delayed-fracture". We have numerically studied the phenomenon of delayed-fracture in Section 5.3, and clarified the important role of fluid diffusion which leads to this phenomenon. In Section 5.4 we reported on our numerical study of fracture in an asymmetric-double-notched sheet specimen of a gel under Mode-I plane-stress loading. This example shows the powerful capability of our gradient-damage theory and its numerical implementation to model the merging of two growing notches.

In this paper we have focused our attention on fracture of an "ideal" single-network polymeric gel with strong chemical crosslinks. It would be useful in the future to extend the theory presented in this paper to interpenetrating-multiple-network gels which incorporate additional non-trivial dissipation mechanisms to toughen polymeric gels (cf., e.g., Gong et al., 2003; Mao et al., 2017a; Zhao, 2014).

Acknowledgements

Support from Exxon-Mobil Research through the MIT Energy Initiative is gratefully acknowledged. We also thank Professor Ju Li (MIT) for providing access to his computer clusters at Xi'an Jiaotong University and MIT, to test the parallelization of our code which helped us complete the simulations whose results are presented in this paper. The help of Dr. Shenghua Wu with some computational aspects of our effort are also gratefully acknowledged.

References

Anand, L., 2012. A cahn-hilliard-type theory for species diffusion coupled with large elastic-plastic deformations. J. Mech. Phys. Solids 60, 1983–2002.
Arruda, E.M., Boyce, M.C., 1993. A three-dimensional constitutive model for the large stretch behavior of rubber elastic materials. J. Mech. Phys. Solids 41 (2), 389–412.
Ayachit, U., The paraview guide: a parallel visualization application, 2015.
Bonn, D., Kellay, H., Prochnow, M., Ben-Djemiaa, K., Meunier, J., 1998. Delayed fracture of an inhomogeneous soft solid. Science 280 (5361), 265–267.
Bouklas, N., Landis, C., Huang, R., 2015. Effect of solvent diffusion on crack-tip fields and driving force for fracture of hydrogels. J. Appl. Mech. 82, 081007.
Bourdin, B., Francfort, G.A., Marigo, J.J., 2000. Numerical experiments in revisited brittle fracture. J. Mech. Phys. Solids 48 (4), 797–826.
Broger, L., Keip, M., Miehe, C., 2017b. Minimization and saddle-point principles for the phase-field modeling of fracture in hydrogels. Comput. Mater. Sci 138, 47–485.
Broger, L., Nateghi, A., Miehe, C., 2017a. A minimization principle for deformation diffusion processes in polymeric hydrogels: constitutive modeling and fe implementation. Int. J. Solids Struct. 121, 257–274.
Brown, H., 2007. A model of the fracture of double network gels. Macromolecules 40 (10), 3815–3818.
Chester, S.A., Anand, L., 2010. A coupled theory of fluid permeation and large deformations for elastomeric materials. J. Mech. Phys. Solids 58 (11), 1879–1906.
Chester, S.A., Anand, L., 2011. A thermo-mechanically coupled theory for fluid permeation in elastomeric materials: application to thermally responsive gels. J. Mech. Phys. Solids 59 (10), 1978–2006.
Chester, S.A., Di Leo, C., Anand, L., 2015. A finite element implementation of a coupled diffusion-deformation theory for elastomeric gels. Int. J. Solids Struct. 52, 1–18.
Doi, M., 2009. Gel dynamics. J. Phys. Soc. Jpn. 78, 052001.
Duda, F.P., Souza, A.C., Fried, E., 2010. A theory for species migration in a finitely strained solid with application to polymer network swelling. J. Mech. Phys. Solids 58 (4), 515–529.
Flory, P.J., 1942. Thermodynamics of high polymer solutions. J. Chem. Phys. 10 (1), 51–61.
Flory, P.J., Rehner, J., 1943. Statistical mechanics of cross-linked polymer networks ii. J Chem Phys 11 (11), 521–526.
Francfort, G.A., Marigo, J.J., 1998. Revisiting brittle fracture as an energy minimization problem. J. Mech. Phys. Solids 46 (8), 1319–1342.
Gaston, D., Newman, C., Hansen, G., Lebrun-Grandie, D., 2009. Moose: a parallel computational framework for coupled systems of nonlinear equations. Nucl. Eng. Des. 239 (10), 1768–1778.
Gong, J., Katsuyama, Y., Kurokawa, T., Osada, Y., 2003. Double-network hydrogels with extremely high mechanical strength. Adv. Mater. 15, 1155–1158.
Gurtin, M.E., 1996. Generalized ginzburg-landau and cahn-hilliard equations based on a microforce balance. Physica D 92 (3–4), 178–192.
Gurtin, M.E., 2002. A gradient theory of single-crystal viscoplasticity that accounts for geometrically necessary dislocations. J. Mech. Phys. Solids 50 (1), 5–32.
Gurtin, M.E., Fried, E., Anand, L., 2010. The Mechanics and Thermodynamics of Continua. Cambridge University Press.
Hong, W., Zhao, X., Zhou, J., Suo, Z., 2008. A theory of coupled diffusion and large deformation in polymeric gels. J. Mech. Phys. Solids 56 (5), 1779–1793.
Huggins, M.L., 1942. Some properties of solutions of long-chain compounds.. J. Phys. Chem. 46 (1), 151–158.
Hui, C., Long, R., Ning, J., 2013. Stress relaxation near the tip of a stationary modei crack in a poroelastic solid. J. Appl. Mech. 80, 021014.
Lake, G.J., Thomas, A.G., 1967. The strength of highly elastic materials. In: Proceedings of the Royal Society of London A: Mathematical, Physical and Engineering Sciences, 300, pp. 108–119.
Lucantonio, A., Nardinocchi, P., Teresi, L., 2013. Transient analysis of swelling-induced large deformations in polymer gels. J. Mech. Phys. Solids 61, 205–218.
Mao, Y., Lin, S., Zhao, X., Anand, L., 2017a. A large deformation viscoelastic model for double-network hydrogels. J. Mech. Phys. Solids 100, 103–130.
Mao, Y., Talamini, B., Anand, L., 2017b. Rupture of polymers by chain scission. Extreme Mech. Lett.
Miehe, C., Schänzel, L.M., 2014. Phase field modeling of fracture in rubbery polymers. part i: finite elasticity coupled with brittle failure. J. Mech. Phys. Solids 65, 93–113.
Miehe, C., Welschinger, F., Hofacker, M., 2010. Thermodynamically consistent phase-field models of fracture: variational principles and multi-field fe implementations. Int J Numer Methods Eng 83 (10), 1273–1311.
Noselli, G., Lucantonio, A., R., M., DeSimone, A., 2016. Poroelastic toughening in polymer gels: a theoretical and numerical study. J. Mech. Phys. Solids 94, 33–46.

Raina, A., Miehe, C., 2016. A phase-field model for fracture in biological tissues. Biomech. Model Mechanobiol. 15 (3), 479–496.
Schröder, J., Neff, P., 2003. Invariant formulation of hyperelastic transverse isotropy based on polyconvex free energy functions. Int. J. Solids Struct. 40, 401–445.
Talamini, B., Mao, Y., Anand, L., 2018. Progressive damage and rupture in polymers. J. Mech. Phys. Solids 111, 434–457.
Tanaka, Y., 2007. A local damage model for anomalous high toughness of double-network gels. EPL (Europhysics Letters) 78 (5), 56005.
Tang, J., Li, J., Vlassak, J.J., Suo, Z., 2017. Fatigue fracture of hydrogels. Extreme Mech. Lett. 10, 24–31.
Treloar, L.R.G., 1975. The Physics of Rubber Elasticity. Oxford University Press, USA.
Wang, X., Hong, W., 2012. Delayed fracture in gels. Soft Matter 8, 8171.
Zhang, T., Lin, S., Yuk, H., Zhao, X., 2015. Predicting fracture energies and crack-tip fields of soft tough materials. Extreme Mech. Lett. 4, 1–8.
Zhao, X., 2014. Multi-scale multi-mechanism design of tough hydrogels: building dissipation into stretchy networks. Soft Matter 10 (5), 672–687.